Wake Effects and Energy Yield Optimization under Realistic Wind Conditions at Ngong Hill Wind Farm

[1*]Omboto, Jane Kwamboka, [1a]Kamau, Joseph Ngugi, [1b]Saoke, Churchill Otieno, and [2]Wekesa, David W.

[1]Department of Physics, Jomo Kenyatta University of Agriculture and Technology, Kenya

[2]Department of Physics, Multimedia University of Kenya, Kenya

DOI: https://doi.org/10.51584/IJRIAS.2026.11030070

Received: 11 March 2026; Accepted: 16 March 2026; Published: 11 April 2026

ABSTRACT

This study evaluates wind resource characteristics, wake effects, layout optimization, uncertainty, and operational strategies using long-term hourly wind data (2010 - 2019) and a one-year validation dataset from the year 2022. The power loss is analyzed using the Jensen wake model, and simulation for power output done with simulations in PYTHON®. The most frequent wind speeds occur within the 4 - 6 m/s range, with a mean extrapolated hub-height wind speed of 9.38 m/s at 50 m. The shape and scale parameters were k = 3.29 and *c* = 9.81 m/s, corresponding to a Betz-adjusted extractable power of 509 W/m², classifying the site as Wind Power Class V at 50 m. Wake modelling showed that the existing layout experiences wake losses of 28.2%, reducing the no-wake Annual Energy Produced (AEP) from 61.86 GWh to 44.41 GWh. Genetic Algorithm-based layout optimization aligned turbine spacing with the dominant wind direction (≥4D along-wind and ≥3D cross-wind), reducing wake losses to 23% and yielding an approximate 5% AEP improvement. Sensitivity analysis demonstrated that ±0.02 variations in the wind shear exponent result in 6–8% changes in AEP, while ±10% perturbations in the Weibull scale parameter produce energy yield variations exceeding ±15%, magnitudes comparable to wake-loss reduction gains. Further, approximately 27% of annual hours occur at wind speeds below 6 m/s, primarily during May-August, as well as during nocturnal and early-morning hours (2100hours - 0300 hours). Maintenance scheduled within these low-wind windows incurs only about 15% of the energy loss associated with maintenance conducted at mean wind conditions, corresponding to an estimated 85% reduction in maintenance-related energy losses. The results demonstrate that maximizing energy yield at Ngong Hills requires a combined strategy integrating aerodynamic layout optimization, uncertainty-aware modelling, and wind-aware maintenance scheduling.

Keywords: Annual Energy Produced; Jensen Wake Model; Maintenance Scheduling; Sensitivity Analysis; Wind Farm Optimization; Wake Effects.

Abbreviations

AEP	Annual Energy Produced
ALIN	Arid Lands Information Network
CI	confidence Intervals
GA	Genetic Algorithms
GIS	Geographical Information System
GWEC	Global Wind Energy Council
IEC	International Electrotechnical Commission

IPCC	Intergovernmental Panel on Climate Change
IRENA	International Renewable Energy Agency
ITCZ	Intertropical Convergence Zone
KenGen	Kenya Electricity Generating Company
LES	Large Eddy Simulation
V_{ci}	Cut-in-speed
V_{co}	Cut-out-speed
V_r	Rated-speed
WRF	Weather Research and Forecasting

INTRODUCTION

The growing global concern over accelerated atmospheric warming driven by greenhouse gas emissions, environmental pollution, and the long-term sustainability of energy resources has intensified interest in renewable and environmentally friendly energy systems. Renewable energy sources, including solar, wind, hydropower, geothermal, and biomass, are increasingly recognized as viable and sustainable alternatives to fossil-fuel-based energy systems due to their low carbon emissions and widespread availability [19], [33]. Among these, wind energy has experienced significant technological advancement and widespread adoption, supported by improvements in turbine design, power electronics, and energy conversion systems [65]. The rapid technological maturity and declining costs of wind power have enabled large-scale deployment, allowing wind energy to contribute a substantial share of national electricity generation in several countries [25], [50]. However, wind power output is inherently dependent on meteorological and geographic conditions, leading to variability and intermittency that are more pronounced compared to some renewable sources such as hydropower. The increasing penetration of wind energy into global electricity markets has resulted in growing volumes of variable renewable generation being integrated into existing power grids. Consequently, concerns have emerged regarding the capability of conventional grid infrastructure to efficiently manage high shares of renewable energy [13]. Given the intermittent nature of wind resources, ensuring grid stability, reliability, and system security has become a critical consideration in modern power system planning and operation [46], [74].

Over the years, a large percentage of Kenya's electric power comes from hydropower plants, which accounted for 45.42% of the total installed capacity in 2020 [52]. Kenya's energy strategy emphasizes the expansion and integration of diverse renewable energy resources; including hydro, geothermal, solar, and wind as part of its approach to achieving national power generation targets and transitioning away from fossil fuels toward a cleaner energy mix [21].

Wake effects are recognized as one of the most significant factors limiting energy yield in wind farms, accounting for losses ranging between 5% and 25% depending on turbine spacing, layout, atmospheric stability, and terrain complexity [48], [65]. Wake effects arise when upstream turbines extract kinetic energy from the wind, resulting in velocity deficits and increased turbulence intensity downstream, which subsequently reduce power output and increase structural loading on downstream turbines [41], [71].

Optimization studies at the global level increasingly employ multi-objective frameworks that balance Annual Energy Production (AEP), wake losses, turbine fatigue loads, and economic metrics. Methods such as genetic algorithms (GA), particle swarm optimization, and gradient-based approaches have been applied to optimize turbine layouts and spacing under wake effects. Recent findings indicate that optimized layouts can improve AEP by 5–15% compared to conventional aligned layouts, particularly in large wind farms [49], [57].

ISSN No. 2454-6194 | DOI: 10.51584/IJRIAS |Volume XI Issue III March 2026

At the regional level, studies across Africa and East Africa highlight the continent's significant wind energy potential while noting persistent challenges related to wake effects in complex terrain and data-scarce settings. Many wind farms operate under suboptimal layouts due to terrain constraints, land-use limitations, and early planning approaches that did not adequately consider wake interactions, with wake losses in African wind farms generally range from 8% to 20%, with higher losses in closely spaced turbines and ridge-top installations, while limited region-specific validation using long-term operational data continues to constrain confidence in yield estimates and optimization strategies [10]. Integrating mesoscale atmospheric models such as the Weather Research and Forecasting (WRF) model with microscale wake models has improved AEP predictions by capturing site-specific wind regimes more accurately [66].

In Kenya, GIS-based analyses have identified several regions with favourable wind potential; however, they note that complex topography and land constraints significantly influence turbine placement and wake behaviour [9]. The Ngong Hills Wind Farm, Kenya's first grid-connected wind power station, has undergone several expansions since its initial commissioning in 1993. As of 2014, its capacity reached 25.5 MW, with plans for further expansion. The site's selection was based on favourable wind regimes observed over a 14-year period, supplemented by data collected between 2006 and 2007, which confirmed its suitability for wind energy generation [37].

Despite its strategic importance as one of Kenya's pioneering wind energy projects, the Ngong Hills Wind Farm, with an installed capacity of approximately 25.5 MW, produces only about 12 GWh of electricity annually, a relatively modest output that suggests a capacity factor substantially below what is technically feasible given the site's wind resource potential [1], [39]. Feasibility data from early development indicated that a 5.1 MW portion of the site alone could generate up to 14.9 GWh per year, pointing to a performance gap that may be attributable in part to wake-induced losses and sub-optimal turbine arrangements under the farm's realistic wind conditions [36], [39]. With plans underway to expand Ngong's capacity through additional phases, there is a timely opportunity to reassess existing layout and control strategies to minimize wake interference and increase AEP. Therefore, a focused analysis of wake effects under realistic local wind regimes is essential for identifying aerodynamic performance losses and for developing evidence-based optimization approaches that can enhance energy yield, improve grid contribution, and align Ngong's output more closely with its resource endowment and Kenya's renewable energy expansion goals.

Furthermore, wind farm performance optimization has traditionally emphasized layout design to reduce wake losses and maximize energy capture, with recent studies demonstrating significant gains in AEP through optimized turbine placement and algorithm selection which includes comparative analyses of layout optimization methods showing measurable improvements in wake loss mitigation [62]. However, while such layout-centric approaches are effective at the design stage, their practical impact for operational wind farms is often limited by physical constraints and site lock-in, leaving operational decision variables, such as maintenance scheduling unaddressed in the energy optimization context. Although research on maintenance scheduling for wind turbines has explored strategies to reduce downtime and maintenance costs, most of this work remains cost- or reliability-focused rather than integrated with wind conditions and energy production optimization for instance preventive maintenance planning that includes potential production loss impact [70]. This study fills this gap by explicitly quantifying and integrating maintenance scheduling as a first-order energy optimization parameter within a unified framework that also incorporates aerodynamic layout optimization and uncertainty-aware wind–wake modelling.

Theoretical Principles

Vertical Wind Shear: Power Law vs Log Law

This is a variation of wind speed with elevation, and describes the change in wind speed as it varies with the height above the ground [34]. To account for differences in measurement heights of the incoming average wind speeds, a wind shear correction was applied for each site, taking into consideration the hub heights of the wind turbine tower. The relationship between wind speed and height can be evaluated using either empirical or theoretical formulations. One commonly applied approach is the power law model [45], expressed in Equation (1)

ISSN No. 2454-6194 | DOI: 10.51584/IJRIAS |Volume XI Issue III March 2026

$$\frac{v_2}{v_1} = \left(\frac{h_2}{h_1}\right)^{\gamma} \quad \ldots\ldots\ldots\ldots\ldots\ldots\ldots\ldots \quad (1)$$

where v_2 and v_1 are wind speeds at heights h_2 and h_1, and γ is the wind shear exponent, which defines the variation of wind speed with height.

Alternatively, vertical wind shear can be evaluated using the logarithmic wind profile, which explicitly accounts for surface roughness effects through the roughness length parameter, (z_o) [34] expressed as equation 2:

$$\frac{v_2}{v_1} = \frac{ln(h_2/z_0)}{ln(h_1/z_0)} \quad \ldots\ldots\ldots\ldots\ldots\ldots\ldots\ldots \quad (2)$$

Recent comparative studies show that while the log law performs better under neutral atmospheric stability, the power law is widely used due to its simplicity, and remains robust for inland sites [48], [66].

The vertical wind shear is an important design parameter, as it directly determines the overall productivity of a wind turbine on a tower of certain height. The shear exponent value used for the extrapolation of wind speed is 0.2, since the site has tall vegetation cover [45]. The wind speeds measured at 10 m height were extrapolated using to shear exponent to 50m heights which is the turbine hub heights at the site.

Wind Distribution

Wind speed is a stochastic quantity. The wind speed for any specified location is represented by density functions. The most common being the Weibull distribution, whose probability density function pd(v) is given in equation 3 as:

$$pd(v) = \frac{k}{c} . \left(\frac{v}{c}\right)^{k-1} . e^{\left(-\left(\frac{v}{c}\right)^{k}\right)} \quad \ldots\ldots\ldots\ldots\ldots\ldots \quad (3)$$

where ***v*** is the wind speed and ***c*** and ***k*** are the scale and shape parameters, respectively; the parameter ***k*** determines the shape the curve takes and ***c*** determines the curve distribution [34]. To analyze a wind regime through the Weibull distribution, it is essential to compute the Weibull parameters ***k*** and ***c*.**

Wind power density, P_d is estimated from the Weibull wind speed distribution [11]:

$$P_d = \frac{1}{2}\rho v^3 \Gamma\left(1 + \frac{3}{k}\right) \quad \ldots\ldots\ldots\ldots\ldots\ldots \quad (4).$$

where, $\boldsymbol{\Gamma}$, is the Gamma function.

2.3 Wind Power Generation

The power available in the wind passing through the swept area of a turbine is given by the kinetic energy flux and is directly proportional to the cube of the wind velocity [64], as expressed in Equation (5):

$$P_{in} = \frac{1}{2}\rho A v^3 \quad (5)$$

where, A is the cross-sectional area of the turbines, V is the wind velocity and ρ is the air density.

However, only a fraction of this power can be extracted by a wind turbine. The total extractable power, P_i of the i^{th} turbine is represented by equation 6:

$$P_i = \frac{1}{2}\rho A_i C_p(\lambda, \beta) v_i^3 \quad \ldots\ldots\ldots \quad (6)$$

Where, ρ is the air density, A_i is rotor swept area of the i-th turbine, $Cp(\lambda,\beta)$, power coefficient, which depends on the tip speed ratio λ and the blade pitch angle β and v_i *is w*ind speed at the i-th turbine. $\boldsymbol{C_p}$ is known as the

ISSN No. 2454-6194 | DOI: 10.51584/IJRIAS |Volume XI Issue III March 2026

Betz coefficient which defines the highest efficiency of any rotor disk type energy extracting device that is placed in the path of flow of a fluid. Using the concepts of conservation of mass, momentum, and energy, Albert Betz, postulated 59.3% of energy as the maximum extractable power for an ideal rotor from a mass of air that is incident at the turbine [34]. Relating equation 5 and 6, C_p is defined as shown in equation 7:

$$C_p = \frac{P_{out}}{P_{in}} \qquad (7)$$

The AEP of the wind farm is calculated by summing the energy produced by all turbines over their respective operating times, as shown in Equation (8):

$$AEP = \sum_{i=1}^{N} P_i \times T_i \qquad (8)$$

P_i is the power output of the *i*-th turbine and T_i is the operating time of the *i*-th turbine.

Wind Variability

Wind variability arises from turbulence across a wide range of spatial and temporal scales, as well as from diurnal, seasonal, and interannual atmospheric processes, which together make accurate prediction of energy capture and the provision of a stable power supply to the grid challenging. Near-surface turbulence and the statistical properties of wind, including rapid short-term fluctuations, strongly influence instantaneous power output and contribute to increased structural fatigue loading on wind [31]. In addition, local factors, particularly terrain/topography and surface roughness associated with vegetation and built environments, significantly modify both the mean wind speed and turbulence structure, leading to substantial spatial variability in wind characteristics between sites [8]. Wind direction is also non-stationary, exhibiting gradual meandering and abrupt shifts over short and long timescales, which can result in yaw misalignment and sustained performance uncertainty ranging from minutes to entire seasons [18].

Turbulence intensity

Atmospheric turbulence arises from the dissipation of kinetic energy in the moving air into thermal energy because of rapid, irregular fluctuations of wind velocity; these fluctuations produce strong short-term variations in instantaneous wind speed even when the hourly (or longer) mean wind speed is relatively steady [59]. Turbulent inflow strongly affects turbine power, wake recovery and structural loads, and is therefore a critical parameter in wind-farm design and operations [63], [69].

Turbulence intensity (TI) quantifies the strength of turbulent fluctuations and is defined as the ratio of the standard deviation of wind speed to the mean wind speed, expressed as:

$$TI = \frac{\sigma_v}{\bar{v}} \quad \ldots\ldots\ldots\ldots\ldots\ldots\ldots\ldots\ldots\ldots (9)$$

Where, $\bar{\boldsymbol{v}}$ is the mean wind speed and $\boldsymbol{\sigma_v}$ is the standard deviation of wind speed computed as:

$$\sigma_v = \sqrt{\frac{1}{N-1}\sum_{i=1}^{N}(v_i - \bar{v})^2} \ldots\ldots\ldots\ldots\ldots\ldots\ldots\ldots\ldots\ldots\ldots\ldots (10)$$

with $\boldsymbol{N}$ the number of samples and $\boldsymbol{v_i}$ the sample at interval *i* [43].

TI varies in space and time because of surface roughness, topography, atmospheric stability (thermal stratification), and mesoscale systems. Small changes in these factors can produce large changes in TI, which explains the strong site dependence and the need to measure or model TI carefully for hub-height assessments. Mesoscale and LES models can estimate TI but have known biases and should be validated against observations [43], [59]. Field and CFD/LES studies show that higher incoming TI typically speeds wake recovery (reducing velocity deficit downstream) but increases unsteady loads and fatigue on turbine components an important aspect for both layout and maintenance planning [63], [69].

ISSN No. 2454-6194 | DOI: 10.51584/IJRIAS |Volume XI Issue III March 2026

Wake Modelling

Wake effects significantly impact wind farm performance by reducing wind velocity downstream of turbines, leading to notable power losses. Accurate modeling of these effects is essential for effective wind farm layout design and energy yield estimation. Wake models can broadly be categorized into computational and analytical approaches. Computational models, while accurate, are often resource-intensive and less suited for iterative layout optimization due to their high computational demands [58].

This study employs the analytical Jensen wake model, to account for wake effects, which are the reductions in wind speed and increases in turbulence caused by upstream turbines affecting downstream turbines. This model builds upon prior research [28], [54]. The schematic representation of the Jensen wake model is illustrated in Figure 1.

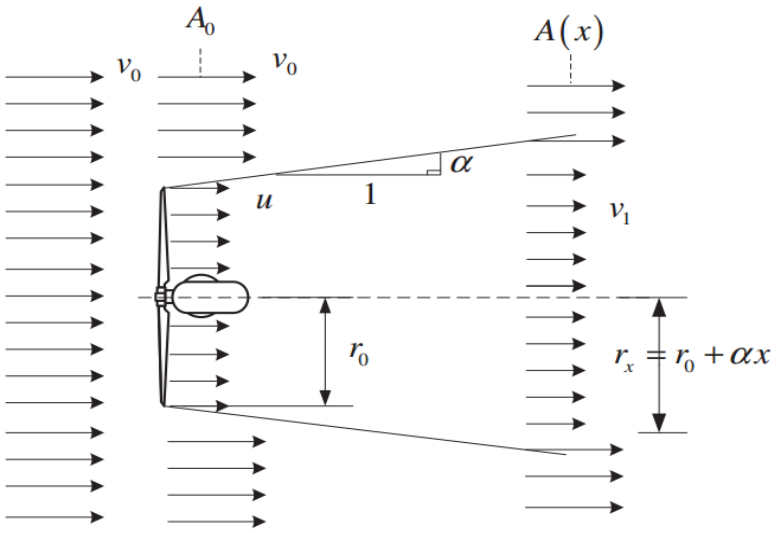

Figure 1: The Schematic representation of the Jensen Wake Model [54].

As illustrated in Figure 1, which presents a schematic representation of the Jensen wake model [54], the turbine wake is assumed to expand linearly with downstream distance from the rotor. This expansion is governed by a wake decay constant, α which reflects the influence of atmospheric conditions and surface roughness on wake recovery. The wake radius r_x at a downstream distance x from the turbine, relative to the rotor radius r_0, is expressed as:

$$r_x = r_0 + \alpha x \quad \ldots\ldots\ldots \quad (11)$$

The Jensen model is a mass-conserving, empirical wake model that estimates velocity deficits downstream of a wind turbine using a linear expansion of the wake radius and a simplified momentum balance [32] as illustrated as:

$$V_x = V_{in}\left[\left\{1 - \left(1 - \sqrt{1 - C_t}\right)\left(\frac{r_o}{r_x}\right)^2\right\}\right] \quad \ldots\ldots (12)$$

where V_{in} (m/s) is the free stream incoming wind speed, V_x (m/s) is the velocity deficit, Ct is thrust coefficient of the turbine.

Uncertainty and Sensitivity in Wind Resource and Wake-Based Energy Assessment

Statistical Representation of Wind Variability and Uncertainty

Wind speed is inherently stochastic, and its variability directly propagates into uncertainty in power density, wake losses, and AEP. Consequently, reliable wind energy assessment requires not only mean values but also statistical descriptors that quantify dispersion and confidence in estimates. The standard deviation (σ) of wind

ISSN No. 2454-6194 | DOI: 10.51584/IJRIAS |Volume XI Issue III March 2026

speed provides a first-order measure of short-term variability around the mean, capturing turbulence intensity and mesoscale fluctuations that influence turbine loading and wake recovery [45], [58].

To quantify the reliability of long-term mean wind speed and derived energy metrics, 95% confidence intervals (CI) are commonly applied under the assumption of approximate normality of annual or multi-year averaged wind speeds. For a sufficiently large dataset, the confidence interval of the mean wind speed, $\bar{v}$ is expressed as:

$$CI = \bar{v} \pm 1.96\frac{\sigma}{\sqrt{n}} \quad (13)$$

where, **σ** is the standard deviation and ***n*** is the number of independent observations. This formulation has been widely adopted in wind resource assessments to quantify uncertainty in extrapolated hub-height wind speeds and AEP estimates [12]. Since wind power scales with the cube of wind speed, even narrow confidence intervals in wind speed translate into substantially wider uncertainty bounds in estimated energy yield [15].

Sensitivity to Wind Shear Exponent (α)

Vertical wind shear is a critical parameter in extrapolating wind speeds from measurement height to turbine hub height, particularly in complex terrain such as Ngong Hills. The power-law shear exponent (α) is known to vary with surface roughness, atmospheric stability, and diurnal heating cycles. Empirical studies report typical α values ranging from 0.10 in offshore or smooth terrain to above 0.30 in forested or complex inland environments [45].

Sensitivity analyses reported in the literature demonstrate that modest variations in α (±0.02–0.05) can lead to 5–15% differences in AEP, especially for turbines operating near rated wind speeds [56], [66]. This sensitivity arises because changes in α alter not only the mean hub-height wind speed but also the frequency distribution of wind speeds relative to the turbine power curve. In wake-affected wind farms, shear also influences vertical wake expansion and recovery, indirectly affecting downstream turbine performance [48].

Sensitivity to Weibull Shape (k) and Scale (c) Parameters

The Weibull distribution parameters play a central role in wind energy estimation. The scale parameter (c) is closely associated with the mean wind speed and strongly governs energy yield [51]. Conversely, variations in k primarily affect capacity factor and wake persistence: lower k values increase the frequency of low-speed operation, which intensifies wake effects and reduces wake recovery rates [6], [58]. Directionally resolved Weibull modelling has been shown to significantly reduce AEP uncertainty in sites with strong directional persistence, such as ridge-top wind farms [14].

METHODOLOGY

The Study Site

The Ngong Wind Farm, the first wind park to be developed in East Africa, is located in Kajiado county in the northern slopes of Ngong Hills at 1°22'51.9"S, 36°38'08.0"E [60]. It comprises thirty wind turbines with a total installed capacity of 25.5 MW: 14 -Vestas (V52/850 kW) installed at a hub height of 49 m; and 16-Gamessa (G52/850 kW) at 55 m; each with a rotor radius of 26 m and name plate capacity of 850 kW. The turbines produce electricity at 690 V, which is initially stepped up to 11 kV at the substation. From there, power transformers boost the voltage to 66 kV for seamless integration into the national grid. The facility houses three power transformers for this purpose [37]. The two turbine models at the site have similar characteristics, therefore for purposes of simulation, power curves for Vestas V52 were used, with operational thresholds of cut-in speed of 3 m/s, rated speed of 12 m/s, and cut-out speed of 25 m/s [61].

Wind data

To evaluate the wind resource potential and estimate the energy output of the Ngong Hills Wind Farm in Kenya, a structured simulation workflow was developed using Python-based data analysis and modelling tools.

ISSN No. 2454-6194 | DOI: 10.51584/IJRIAS |Volume XI Issue III March 2026

This study utilized a 10-year dataset of hourly wind speed and direction, recorded between January 2010 and December 2019. The data were obtained from the KenGen, which operates the Ngong Hills Wind Power Station. To ensure the accuracy of historical extrapolations, this dataset was validated using ground-level wind measurements recorded at 10 meters above ground level for the entire year of 2022. Wind data were collected using calibrated meteorological instruments installed at the Ngong wind farm, with wind speed and direction measured at 10 m above ground level and recorded at hourly intervals. The dataset provided long-term coverage and was quality-controlled prior to analysis, with wind-speed and directional uncertainties assumed to be within ±0.2 m/s and ±2°, respectively. The processed data were extrapolated to hub height of 50 m and used for turbulence intensity estimation, wake modelling, and AEP assessment.

A limitation of this study is the reliance on a one-year validation dataset (2022) to complement the primary 10-year wind resource analysis (2010–2019), from which wake losses and AEP estimates are derived.

Data Acquisition and Preprocessing

The primary dataset comprised hourly wind speed and direction measurements in CSV format, including timestamps, wind speed (m/s), and direction (degrees). Initial data preprocessing involved the handling of missing values using linear interpolation techniques to maintain the temporal continuity of the dataset. To ensure the integrity of the wind speed data, outliers, specifically values below 0.5 m/s and above 30 m/s, were removed in accordance with the IEC 61400-12-1 standard for power performance measurements of electricity-producing wind turbines [33]. Wind direction values were standardized to fall within the 0°–360° range, wind direction was expressed in degrees clockwise from true North as 0° or 360°, for uniformity in directional analysis Wind data spanning at least one year were collected for each site, including wind speed and direction at multiple measurement heights. Wind roses were generated to identify predominant wind directions across the proposed layout area. Additionally, one month of field measurements validated wind atlas data. Directional frequency data were binned into 60° sectors, and mean wind speeds were calculated within each sector to support directional-aware analysis.

Vertical Wind Shear Extrapolation

Wind speed measurements were originally available at a reference height of 10 m and therefore required extrapolation to turbine hub heights of 49 m and 55 m. This extrapolation was performed using the power-law wind shear illustrated in Equation 1, with a shear exponent $\alpha \approx 0.20$. The shear exponent was obtained using a log–log linear regression between concurrent wind speed measurements at 10 m and 49 m, rather than a simple arithmetic average. Specifically, α was estimated from the slope of the linear fit to $\ln(v)$ versus $\ln(z)$ over the period of concurrent measurements, yielding a single representative exponent that minimizes least-squares error across the available dataset.

Due to the limited availability of continuous multi-height measurements, the derived value is treated as a representative site-specific estimate rather than a fully resolved statistical wind shear model. The selected exponent produced physically consistent vertical wind profiles and was subsequently applied to extrapolate wind speeds to additional hub heights of 45 m, 65 m, and 90 m for comparative analysis.

To enhance projection reliability, the extrapolation framework also accounted for site-specific surface roughness and terrain characteristics, reflecting the complex topography of the Ngong Hills. The chosen shear exponent is consistent with values reported for terrains with moderate surface roughness, including grassy slopes and sparsely forested landscapes [12]. Recognizing the inherent uncertainty associated with shear assumptions, particularly in complex terrain, the robustness of this representative α was evaluated through a sensitivity analysis in which α was varied within a plausible range (±0.03–0.05) consistent with observed terrain roughness classes.

Wind Speed Distribution Modelling

To understand the statistical characteristics of the wind regime, in each directional sector, at the extrapolated heights wind speed distributions were fitted using the two-parameter Weibull model equation. The Weibull distribution, with its shape (k) and scale (c) parameters, was estimated using maximum likelihood methods,

ISSN No. 2454-6194 | DOI: 10.51584/IJRIAS |Volume XI Issue III March 2026

which are commonly applied in wind resource assessments due to their robustness and accuracy [55]. This analysis was essential for estimating the frequency of wind speeds near the turbine's rated speed, which directly affects energy yield. Assigning individual Weibull distributions per wind direction improved energy output modelling accuracy compared to isotropic assumptions.

Power Output Modelling and Energy Estimation

The estimation of power output and AEP for the optimized wind farm followed a structured, two-stage modelling framework. First, hub-height wind speeds at 49 m and 55 m were converted into turbine-specific power output using the manufacturer's power curve for the Vestas V52 (850 kW) wind turbine. Second, wake-induced wind speed deficits across the turbine array were incorporated using the Jensen wake superposition model to provide a realistic representation of turbine interactions and downstream performance losses.

Wind power density was first estimated from the Weibull distribution using equation 4, defining the site's theoretical energy potential. AEP was then computed by integrating the turbine power curve with the hub-height wind speed distribution, incorporating wake-induced velocity deficits via the Jensen model.

Wind Speed–Power Output Mapping

Wind speeds measured at the relevant hub heights were transformed into electrical power output through a piecewise function derived from the operational characteristics of the Vestas V52 turbine. The turbine operates within three key thresholds:

i. Cut-in speed (V_{ci}): 4 m/s, below which no electricity is produced;

ii. Rated speed (V_r): 14 m/s, above which the output is capped at the rated 850 kW;

iii. Cut-out speed (V_{co}): 25 m/s, where the turbine automatically shuts down for safety.

Between the cut-in and rated wind speeds, power output was modelled using a cubic relationship with wind speed, as shown in equation 6. Additionally, this followed the standard four-region operational model widely applied in wind turbine analysis [15], [30]. These regions correspond to different aerodynamic and operational behaviours: Region I (no production below cut-in), Region II (cubic power increase), Region III (constant rated output), and Region IV (shutdown above cut-out) as illustrated in Figure 2.

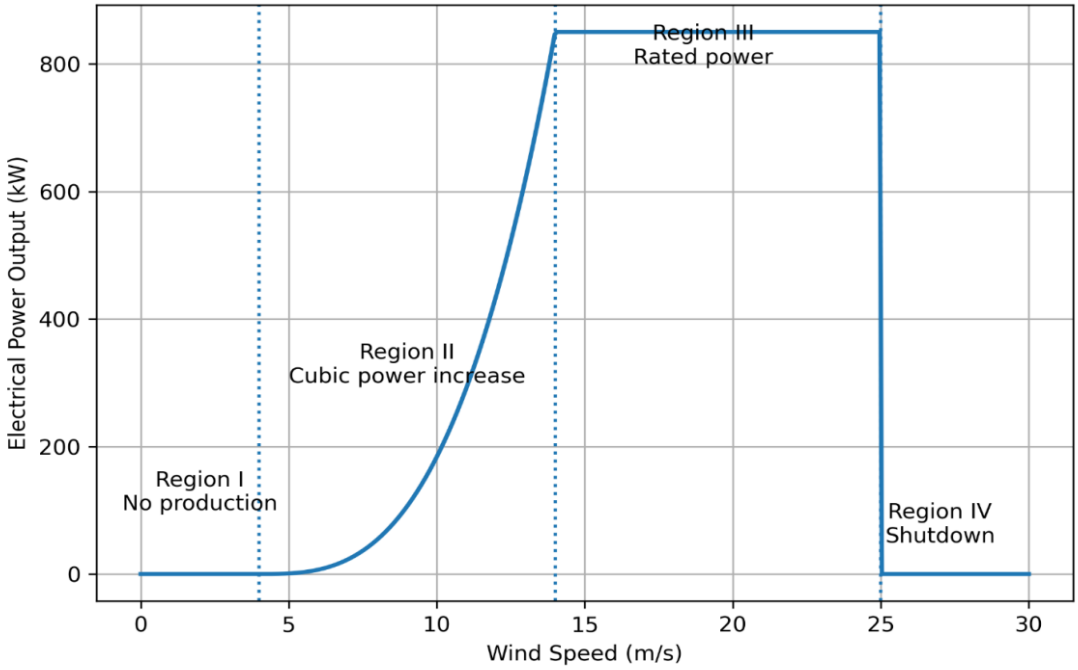

Figure 2. Recreated Power Curve for the Vestas V52 based on published Vestas' datasheets.

ISSN No. 2454-6194 | DOI: 10.51584/IJRIAS |Volume XI Issue III March 2026

Figure 2 represents the four distinct regions for VestasV52 turbines power curve. Following classical aerodynamic theory, power in Region II increases proportionally to the cube of wind speed, reflecting the cubic dependence of wind power on velocity [30]. The turbine power curve was implemented using the following piecewise function:

$$P(V) = \begin{cases} 0, & V < V_{ci} \\ P_{rated}\left(\frac{V^3 - V_{ci}^3}{V_r^3 - V_{ci}^3}\right), & V_{ci} \le V < V_r \\ P_{rated}, & V_r \le V \le V_{co} \\ 0, & V > V_{co} \end{cases} \quad \ldots\ldots\ldots\ldots\ldots\ldots\ldots\ldots (14)$$

The equation 14 ensured a smooth transition from zero output at cut-in to full output at rated speed, while accurately representing the turbine's-controlled power-limiting behaviour above the rated wind speed. The cubic interpolation between cut-in and rated speeds provides a realistic approximation of partial-load performance and is widely used in simulation-based energy assessments [15], [30]. At each timestep or wind-speed bin, the hub-height wind speed was supplied to the function to generate instantaneous power output, which was later integrated into the AEP calculation.

Wake Loss Modelling

Wake effects across the wind farm were quantified using the Jensen wake superposition model, which estimates downstream velocity deficits using Equation 12 by modelling the expansion of the wake cone and the reduction of wind speed behind each turbine. The model was applied to each candidate layout to generate wake-adjusted wind speeds for power calculations.

The Jensen wake model is extensively used in analytical wind farm studies due to its computational efficiency and ease of implementation, though these advantages stem from simplifying assumptions that limit predictive accuracy. The model assumes a steady, one-dimensional wake with a uniform "top-hat" velocity deficit that expands linearly downstream, neglecting the radial velocity variation observed in real wakes. Empirical studies show that Gaussian or cosine-shaped profiles more accurately represent wake recovery, particularly in the near-wake region [17], [73]. As a result, the Jensen model may misrepresent peak deficits and wake boundaries, especially in closely spaced turbine layouts.

Additionally, the Jensen model does not explicitly account for wake-added turbulence, cross-stream or vertical velocity components, or atmospheric variability, and is based on mass conservation rather than full momentum conservation. These simplifications constrain its ability to capture wake recovery under varying inflow conditions and can lead to underestimation of cumulative wake losses compared to higher-fidelity models [26], [67].

Despite these limitations, the Jensen model remains well suited for large-scale layout optimisation and preliminary assessments, where computational efficiency and robustness are critical. Compared to alternative analytical models, it offers a practical balance between accuracy and cost. The Frandsen model incorporates wake-added turbulence but is primarily applied to structural load analysis and introduces greater parameter sensitivity [22], while the Bastankhah Gaussian model provides improved wake representation at the expense of higher computational demand and calibration requirements [6], [16]. Given the trade-off between model fidelity and efficiency, the Jensen model is an appropriate choice for comparative layout analysis and wake-loss estimation within the scope of this study.

Because all turbines in the study comprised the same Vestas V52 model, a uniform hub height of 50 m was maintained throughout the analysis. This ensured that optimization efforts remained focused on horizontal turbine spacing and spatial configuration, the primary controllable factors for reducing wake losses given a homogeneous turbine fleet.

ISSN No. 2454-6194 | DOI: 10.51584/IJRIAS |Volume XI Issue III March 2026

Inter-Turbine Distance Variation for Wake Reduction

Layout optimization was carried out by systematically varying the spacing between turbines while keeping all turbines within the farm boundary. The GA treated each turbine's **(**x, y**)** position as a continuous decision variable, enabling flexible repositioning within allowable limits. To ensure engineering feasibility and safety, spacing constraints were applied:

- Along-wind spacing (parallel to NE–ENE dominant wind direction)**:** 4D to 10D
- Cross-wind spacing (perpendicular to NE-ENE direction): 3D to 6D.

These ranges align with recommended industry guidelines for reducing wake overlap while limiting excessive land-use expansion.

The GA explored thousands of potential layouts by applying random initial placement, crossover, and mutation operations. Layouts that resulted in turbines being placed too close along the prevailing wind axis exhibited high wake deficits and were automatically penalized. Conversely, layouts that increased cross-wind spacing, staggered turbine rows, or avoided linear alignment with the NE–ENE inflow were rewarded and carried forward through subsequent generations.

Integration with the Wake Model

For each candidate layout, the GA-Jensen wake model calculated:

- the magnitude of wake-induced velocity deficits across the layout,
- the overall wake loss percentage for the farm, and
- the resulting AEP of the configuration.

The GA iteratively refined the turbine positions to minimize total wake losses while maximizing AEP. Through successive generations, this process converged toward an optimized layout that significantly reduced wake overlaps along the NE–ENE inflow direction.

Annual Energy Production Computation

AEP was computed by integrating power output across the wind speed frequency distribution for each turbine location, using both free-stream and wake-adjusted wind speeds. Turbine-level AEP values were aggregated to obtain the total farm-level AEP under two conditions:

i. ideal (no-wake) scenario, representing theoretical maximum energy yield; and

ii. realistic (wake-influenced) scenario, representing actual expected performance.

The difference between these two scenarios provided the wake-loss percentage for the layout.

Genetic Algorithm–Based Wind Farm Layout Optimization

Wind farm layout optimization was performed using a **GA** implemented in PYTHON®, version 3.12, with the objective of maximizing AEP while minimizing wake-induced power losses**.** The optimization problem is formulated through a multi-objective fitness function that balances energy maximization and wake loss reduction. The total extractable power of the wind farm is defined by Equation (6), while AEP is computed as the cumulative AEP of all turbines illustrated in Equation (8). Wake losses are quantified as the difference between ideal and wake-affected turbine power output:

$$\boldsymbol{Wake\ Losses} = \sum_{i=1}^{N}\left(\boldsymbol{P_{ideal,i}} - \boldsymbol{P_{actual,i}}\right) \qquad (15)$$

$P_{\text{ideal},i}$ is the expected power output of the i-th turbine in the absence of wake effects and $P_{\text{actual},i}$ is the power output of the i-th turbine considering wake effects.

Layout Representation and Fitness Evaluation

Each layout L_j in the population is represented as a set of turbine positions within the farm boundary:

$$\boldsymbol{L_j} = \{(\boldsymbol{x_1}, \boldsymbol{y_1}), (\boldsymbol{x_2}, \boldsymbol{y_2}), \ldots, (\boldsymbol{x_m}, \boldsymbol{y_m})\} \qquad (16)$$

Where: (x_i, y_i) are the coordinates of the i-th turbine in the wind farm and m, is the number of turbines in the layout.

The fitness function $f(L_j)$ evaluates the performance of each layout by combining AEP and wake losses:

$$\boldsymbol{f(L_j) = AEP(L_j) - \alpha. Wake\ Losses(L_j)} \qquad (17)$$

Where, α, is a weighting factor that balances the importance of maximizing AEP versus minimizing wake losses.

3.4.1 Genetic Algorithm Operators

The GA optimization proceeds iteratively through standard evolutionary operators:

***Population Initialization**:* An initial population of N layouts is generated randomly within the wind farm boundary, ensuring feasibility with respect to spacing and boundary constraints.

***Selection**:* Tournament selection is used to select parent layouts based on fitness values to create the next generation. The probability $P(L_j)$ of selecting layout L_j is proportional to its relative fitness:

$$\boldsymbol{P(L_j)} = \frac{f(L_j)}{\sum_{k=1}^{N} f(L_k)} \qquad \ldots\ldots\ldots \quad (18)$$

Crossover: Offspring layouts are generated by recombining turbine coordinates from two parent layouts *Lp* and *Lq* to produce offspring layouts, a simple crossover operation can be represented as:

$$L_{offspring} = \{(x_1, y_1), \ldots, (x_k, y_k)\} \cup \{(x_{k+1}, y_{k+1}), \ldots, (x_m, y_m)\} \quad \ldots\ldots\ldots\ldots\ldots\ldots \quad (19)$$

where, the first k turbine positions are taken from *Lp*, while the remaining $m{-}k$ turbine positions are taken from *Lq.*

Constraints and Termination Criteria

The optimization is subject to the following constraints:

Turbines must lie within the wind farm boundary:

$$(\boldsymbol{x_i}, \boldsymbol{y_i}) \in \boldsymbol{Boundary}\ \forall \boldsymbol{i} \quad \ldots\ldots\ldots\ldots\ldots\ldots\ldots\ldots\ldots\ldots.. (20)$$

Minimum spacing between turbines must satisfy:

$$\sqrt{(\boldsymbol{x_i} - \boldsymbol{x_j})^2 + (\boldsymbol{y_i} - \boldsymbol{y_j})^2} \geq \boldsymbol{D_{\min}} \quad \forall \boldsymbol{i} \neq \boldsymbol{j} \quad \ldots\ldots\ldots\ldots\ldots\ldots\ldots..(21)$$

The total number of turbines is limited by the number of turbines at the Ngong wind farm.

$$\boldsymbol{N \leq N_{max}} \qquad \ldots\ldots\ldots\ldots\ldots\ldots\ldots\ldots\ldots\ldots\ (22)$$

Constraint violations are handled through rejection and penalization to ensure physically feasible layouts. The GA was executed with 20–50 layouts per generation**,** a mutation rate of 1–3%**,** and up to 20 generations per

ISSN No. 2454-6194 | DOI: 10.51584/IJRIAS |Volume XI Issue III March 2026

scenario, following parameter recommendations by [20] & [42]. Convergence was assessed based on stabilization of the best fitness value across successive generations.

Simulation Setup

The simulation setup involved defining the wind farm area, turbine configurations, and wind conditions. The wind farm area was set to 800,000 m². The wind conditions, including wind speed and direction, were based on historical data from the Ngong Hills site. The simulation was run for 20 generations, with each generation consisting of 20 layouts. The best-performing layouts from each generation were carried over to the next generation, and new layouts were generated through crossover and mutation. The simulation continued until the optimal layout was found, or the maximum number of generations was reached. The overall optimization workflow is illustrated in Figure 3, which summarizes the iterative process of selection, crossover, mutation, and evaluation.

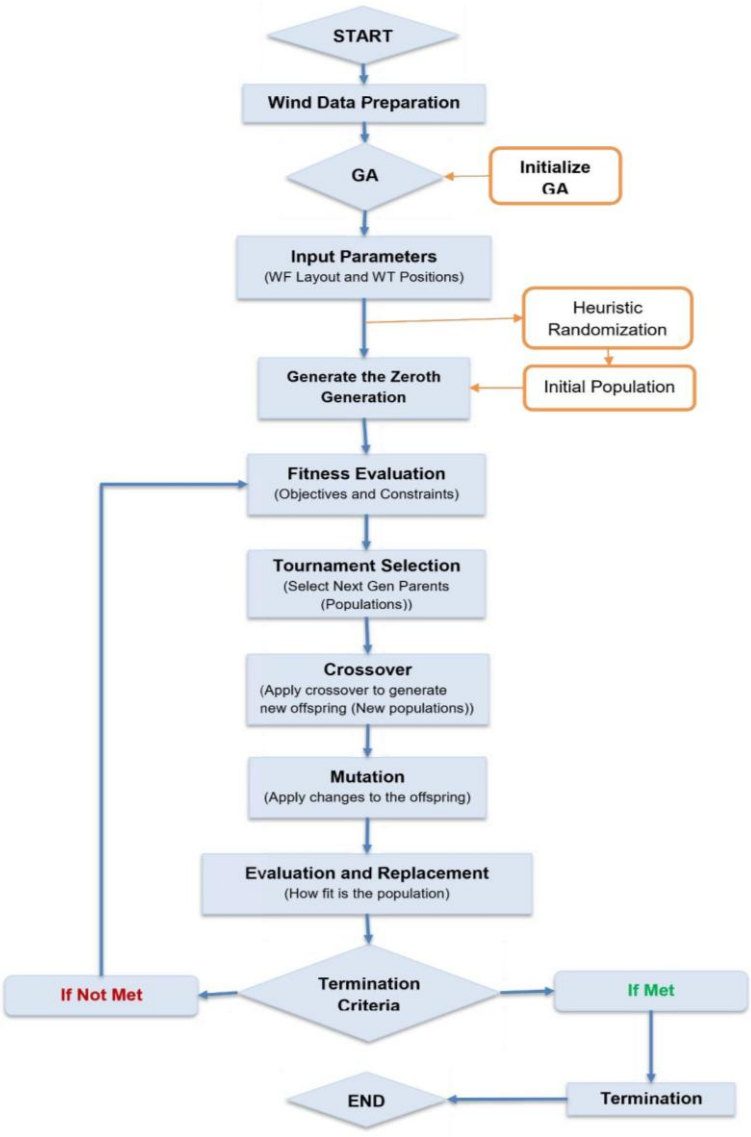

Figure 3: Flow Chart of the GA.

The GA–based optimization workflow is summarized in Figure 3, which illustrates the iterative coupling between layout generation, wake modelling, and fitness evaluation. As shown, the process begins with the initialization of feasible turbine layouts within the wind farm boundary, followed by evaluation of each layout using an objective function that combines AEP and wake-induced power losses computed with the Jensen model. High-performing layouts are then selected and evolved through crossover and mutation, enabling systematic exploration of the spatial search space while maintaining population diversity. The resulting layouts are re-evaluated under identical wind and wake conditions, completing one evolutionary cycle. This loop is repeated across successive generations until convergence is achieved, as

ISSN No. 2454-6194 | DOI: 10.51584/IJRIAS |Volume XI Issue III March 2026

indicated by stabilization of fitness values or attainment of the maximum number of generations, thereby ensuring consistent identification of layouts that maximize energy yield while minimizing wake losses.

Uncertainty Quantification and Sensitivity Analysis Framework

Standard Deviation and Confidence Interval Estimation

For each wind speed time series at hub height, the mean wind speed and standard deviation were computed. Assuming statistical independence at hourly resolution over multi-year periods, 95% confidence intervals were derived for mean wind speed and propagated through the power curve to estimate uncertainty bounds on turbine-level and farm-level AEP. This approach aligns with IEC 61400-12-1 recommendations and has been applied in several empirical wind farm performance studies [12].

Sensitivity Analysis of Wind Shear, Shape and Scale Parameters

A parametric sensitivity analysis was conducted by systematically perturbing α, k, and c around their baseline values while holding turbine layout and wake model parameters constant. The following ranges, consistent with values reported in the literature for inland African sites, were considered:

- Shear exponent (α): ±0.02 and ±0.05
- Weibull scale parameter (c): ±5% and ±10%
- Weibull shape parameter (k): ±10%

For each perturbation, wind speeds were re-extrapolated, wake-adjusted velocities recomputed using the Jensen model, and AEP recalculated. This approach isolates the contribution of atmospheric and statistical uncertainty from layout-induced wake effects, following best practice in wind energy uncertainty analysis [48], [57].

Wind-Aware Maintenance Scheduling

The maintenance scheduling is based on the principle that energy losses during turbine downtime depend strongly on the prevailing wind speed at the time maintenance is conducted. For a fixed maintenance duration, energy loss is proportional to the expected power output under the wind conditions during the maintenance window. By shifting planned maintenance activities from high-wind to low-wind periods, total energy losses can be significantly reduced without altering turbine availability or operational strategy.

Hourly wind-speed data were analysed to identify representative average-wind and low-wind conditions at the site. Average-wind conditions (v_{avg}) were defined using the long-term mean wind speed, while low-wind conditions (v_{low}) were selected from the lower tail of the wind-speed distribution, corresponding to nocturnal and seasonal low-production periods identified in the Results section. These periods are characterised by reduced AEP contribution and elevated turbulence intensity, making them suitable candidates for scheduled maintenance.

Energy loss due to maintenance downtime was estimated assuming a fixed maintenance duration T_m identical for both baseline and optimized scenarios. The expected energy loss E_{loss} during maintenance was calculated as:

$$E_{loss} = P(v)T_m \quad \ldots\ldots\ldots\ldots 23$$

where $P(v)$ is the turbine power output evaluated from the manufacturer's power curve at the representative wind speed v.

Two scenarios were considered: maintenance conducted during average-wind conditions ($v = v_{avg}$), and maintenance shifted to low-wind conditions ($v = v_{low}$).

ISSN No. 2454-6194 | DOI: 10.51584/IJRIAS |Volume XI Issue III March 2026

The relative reduction in maintenance-related energy loss was then expressed as:

$$Reduction\ \% = \left(1 - \frac{P(v_{low})}{P(v_{avg})}\right) \times 100 \quad \ldots\ldots\ldots\ldots\ldots\ldots\ldots\ldots\ 24$$

Model Calibration and Validation

The model was validated using independent wind measurements recorded in 2022 at 10 meters above ground level., ensuring that the simulations accurately represent real-world conditions, by comparing the simulated power output and wake effects with actual data from the Ngong Hills wind farm. The validation process involved running the model with the same turbine configurations and wind conditions as those present at the Ngong Hills site. The results showed a close match between the simulated and actual power outputs, confirming the accuracy of the model in predicting wind farm performance.

RESULTS AND DISCUSSION

Mean Wind Speed

The assessment of the wind potential at the chosen location involved an analysis of wind characteristics, including wind speed, prevailing direction, duration, availability, and the resulting power density. By using the measured frequencies, the frequency distribution of wind speed and direction was obtained and represented as shown in Figure 4.

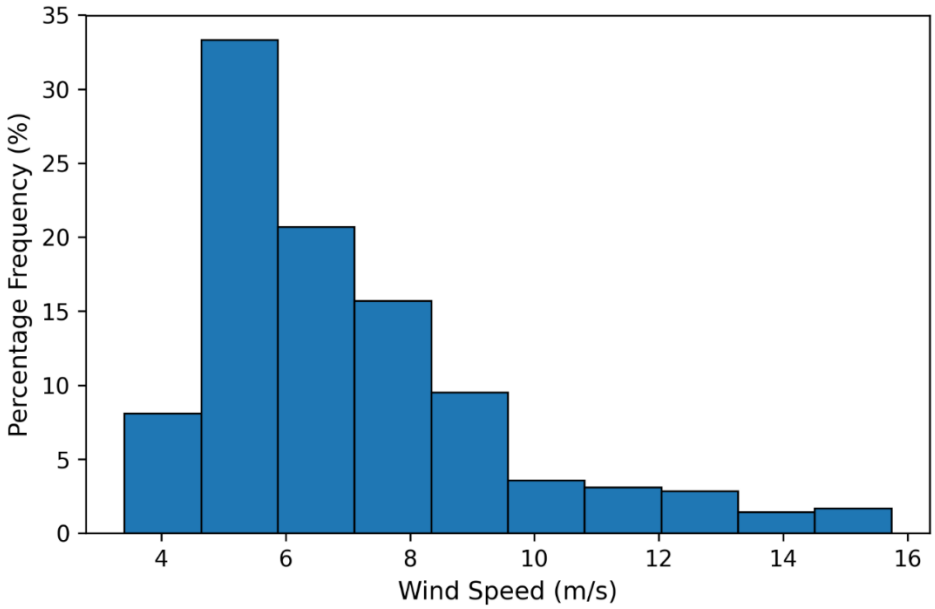

Figure 4: Wind Speed Distribution

Figure 4 shows that the wind speed distribution at the study site is dominated by moderate winds, with the highest percentage frequency occurring between 4 m/s and 6 m/s, indicating that these speeds are the most prevalent within the dataset. This range aligns with many wind regimes considered marginal to moderately strong for wind energy applications, where turbines begin generating power but may not yet reach rated output. The occurrence of higher wind speeds declines rapidly, and very high wind speeds (14 m/s to 16 m/s) are rare in this dataset. This limited occurrence of extreme winds is consistent with commonly observed wind speed distributions, which are typically characterized by a dominant mode at moderate wind speeds and a long tail toward higher values; such right-skewed distributions vary geographically in response to local climatic conditions and terrain effects and generally exhibit low frequencies of high wind speed events [55].

Using the power-law extrapolation provided in Equation (1), the mean wind speed at 50 m hub height was estimated to be 9.38 m/s with a standard deviation of 3.46 m/s. The extrapolated maximum and minimum at 50

ISSN No. 2454-6194 | DOI: 10.51584/IJRIAS |Volume XI Issue III March 2026

m were 17.1 m/s and 2.1 m/s, respectively. A mean wind speed of ~9 m/s is within the operational sweet spot for many onshore wind turbines, which typically achieve near-rated performance between approximately 8 m/s and 12 m/s. Practical wind turbines typically begin generating measurable power at wind speeds of around 3 m/s (Früh, 2023), reaching rated output around 10–13 m/s and shutting down above approximately 25 m/s to prevent mechanical damage (cut-out speed) [72].

Wind Speed Variability

The variations for wind energy characteristics for hourly and daily situations for wind speed at the Ngong wind farm were established and the information represented in time series graphs. These variations in wind speed for the year 2022 with 0000 hours and the month of January as the reference are represented in Figures 5 (a) and (b) respectively.

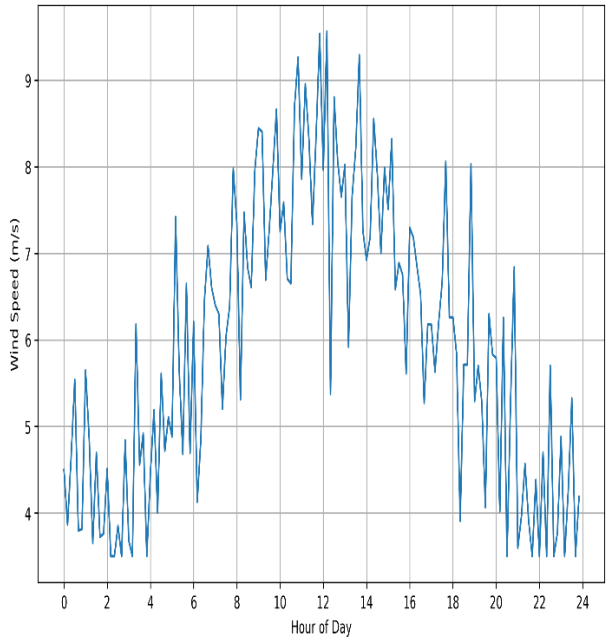

Figure 5(a): Diurnal Wind Speed

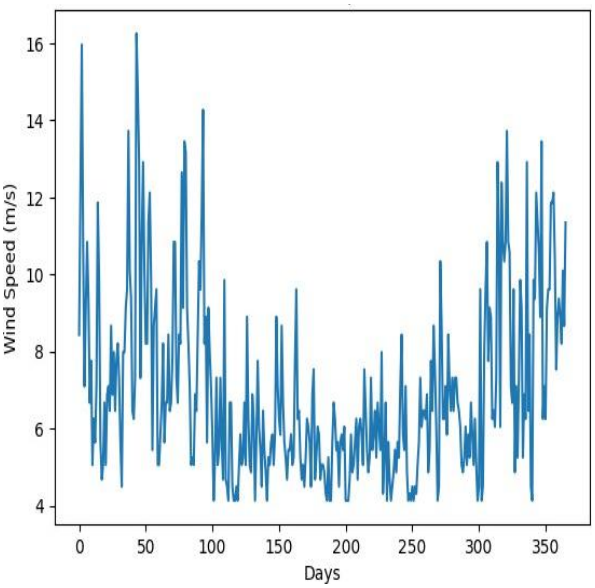

Figure 5 (b): Wind Speed Variation

The time-series patterns of wind speed presented in Figures 5(a) and 5(b) reveal a strongly seasonal and turbulent wind regime, shaped by both large-scale atmospheric processes and local terrain effects. The diurnal wind speed profile in Figure 5(a) indicates that the lowest wind speeds occur between 2100 and 0300 hours,

ISSN No. 2454-6194 | DOI: 10.51584/IJRIAS |Volume XI Issue III March 2026

which imply lower energy generation during this time, after which a gradual increase in wind speed is observed toward daytime, accompanied by higher variability. This pattern is consistent with atmospheric boundary layer theory, where nocturnal radiative cooling leads to a stable layer that suppresses vertical mixing and reduces near-surface wind speeds [5].

Similarly, wind speeds fluctuate significantly between 4 m/s and 16 m/s throughout the year. Figure 5(b) indicate that speeds are relatively lower during the period from May to August, highlighting a distinct seasonal minimum within the annual cycle. Critically, while some regions experience stronger monsoonal winds during this period, the observed reduction suggests site-specific atmospheric controls, such as localized stability, terrain effects, and weakened synoptic forcing, which can limit wind acceleration despite seasonal changes [44]. In practical terms, the clustering of low winds mid-year implies seasonal variability in AEP and capacity factor, implying relying solely on annual averages will result in much reduced values of the AEP and capacity factor, which have a big discrepancies with the individual monthly mean averages [15].

The observed patterns align with previous studies on Kenyan inland wind regimes, which similarly report strong seasonal modulation and high intra-seasonal variability due to ITCZ dynamics and complex terrain [35]. However, the higher directional spread observed here suggests a slightly more turbulent and multi-modal wind climate compared with coastal sites. The recurring patterns suggest seasonal variations influenced by meteorological factors and turbulence [45].

Wind Direction

A wind rose diagram is a useful diagram which illustrates wind speed frequency and wind direction all together in one diagram [45]. Analyzing the wind direction is useful for understanding the wake effect, which turbines could be on the path of the other turbines which could result in a reduction of wind speed. Wind speed rose, provides appropriate knowledge on the predominant wind direction of the site which is a vital factor in determining the direction from which maximum possible wind energy can be harnessed. The observed wind direction for entire 2022 were organized at varying intervals for wind speed for each direction was analyzed and represented in Table 1.

Table 1: Directional Distribution of Wind Speed Characteristics

	N	**NE**	**E**	**SE**	**S**	**SW**	**W**	**NW**
Count	60	1568	9890	1021	28	144	86	47
cumulative	112.9	12567.4	97805.6	10075.8	61.6	446.7	187.3	72.5
Average	1.88	8.02	9.89	9.87	2.2	3.10	2.17	1.54

Table 1 presents the directional distribution of wind speed observations, including the number of occurrences, cumulative wind speed, and mean wind speed for each compass direction. The results show a strong directional dependence of the wind regime at the site. Winds from the east (E) and southeast (SE) directions dominate both in frequency and magnitude, accounting for the highest number of observations and the largest cumulative wind speed values. These directions also exhibit the highest mean wind speeds, with averages of 9.89 m/s (E) and 9.87 m/s (SE).

In contrast, winds from the north (N), south (S), west (W), and northwest (NW) occur infrequently and are characterized by relatively low mean wind speeds, generally below 3 m/s. The northeast (NE) direction shows a moderate number of observations with an average wind speed of 8.02 m/s, while the southwest (SW) exhibits moderate wind speeds but limited occurrence.

By studying the hourly wind roses can help determine the best location for the wind turbines. The wind rose for the site is given in the Figure 6.

ISSN No. 2454-6194 | DOI: 10.51584/IJRIAS |Volume XI Issue III March 2026

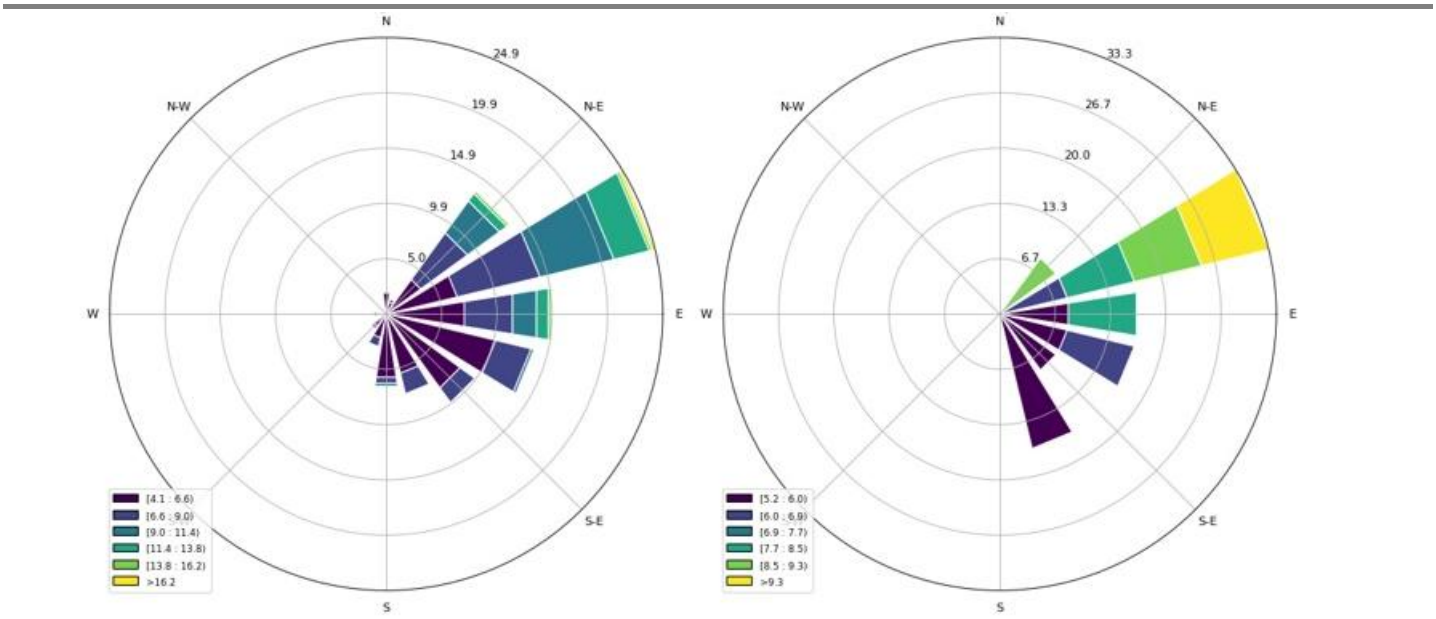

Figure 6: Wind Rose Diagrams for observed wind direction of the entire 2022

The wind rose diagrams for the Ngong wind farm illustrated in Figure 6 provide a clear depiction of the prevailing wind regimes over 2022, using both daily and monthly mean values. Across both temporal resolutions, the site shows a highly consistent directional pattern, with winds predominantly blowing from the northeast (NE) through east-northeast (ENE). This persistent inflow is strongly indicative of the stable large-scale atmospheric controls influencing the region, particularly the Turkana Jet and the channeling of trade winds between the Kenyan highlands and the Great Rift Valley, features known to sustain recurrent north-easterly flows across northern and central Kenya [40].

In the daily mean wind rose, the highest frequency of occurrence is concentrated within the 6.0–9.0 m/s speed class from the NE direction. The relatively narrow petals in this diagram reflect that on most days, winds arrive from a tightly confined directional sector with moderately strong speeds. In contrast, the monthly mean wind rose displays broader and longer petals in the same NE–ENE sectors and extends more prominently into higher wind speed classes (≥9 m/s). This indicates that when winds are aggregated over longer periods, intermittent episodes of stronger winds become more visible, revealing greater inter-month variability than what is captured in day-to-day averages. Such behaviour aligns with the seasonal modulation of the Turkana Jet and associated monsoon systems ([40].

Despite these differences in speed representation, the strong directional similarity between the daily and monthly charts highlights the high directional stability of the site. This is advantageous for wind farm design, as predictable inflow directions facilitate optimized turbine alignment, reduced wake effects, and overall enhanced energy capture. The key distinction lies in how each temporal scale represents wind speeds: daily means emphasize the most frequently occurring moderate winds, whereas monthly means capture the cumulative influence of less frequent but more powerful wind events, which often contribute disproportionately to AEP [27].

Overall, the dominance of NE–ENE winds and frequent 6–9 m/s occurrences confirm Ngong as a favourable wind energy site, offering predictable directional flows and sufficient wind speeds to support efficient turbine operation and optimized farm layout.

Probability Density Function

The average wind speed of the site is not sufficient to fully understand the available wind potential. To overcome the unpredictability of wind characteristics, a statistical analysis was deemed essential, consequently, Weibull distribution model was used. Weibull model shape parameter *k,* and scale parameter, *c,* were determined from the data and the respective distribution curves drawn as illustrated in Figure 7.

ISSN No. 2454-6194 | DOI: 10.51584/IJRIAS |Volume XI Issue III March 2026

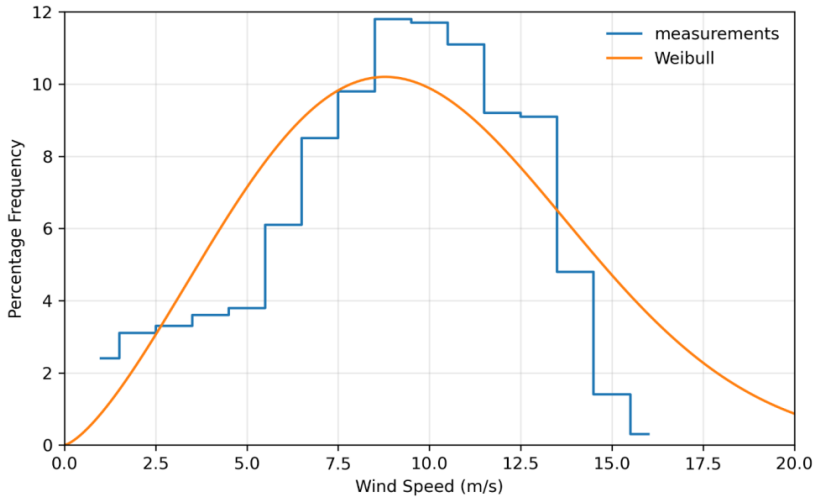

Figure 7: Wind Distribution Curve

The Figure 7 illustrates the probability density function which shows the probability of occurrence of each observed wind speed. Weibull probability density curve provide the ability of determining likelihood of wind blowing at a certain speed in any given time [34]. The curve is unimodal, peaking at a wind velocity of about 9 m/s, indicating this as the most common wind speed, which is near the mean wind speed of 9.38 m/s. Probability decreases for wind speeds lower or higher than this peak, which shows that the wind speed is more likely to be near the average value than significantly different from it, and it has an almost equal chance of being lower or higher than the average [45].

Power Density

The scale and shape parameters were also used to calculate the site's localized power density. The shape and scale parameters of 3.29 and 9.81m/s respectively and the site's air density whose value is 1.29g/l were used which gave a theoretical power density of 858W/m^2. This power was noted to be almost the same as calculated power if the wind was blowing at the average speed of 9.38 m/s. To achieve the maximum power that can be extracted, Betz's limit was taken into consideration, which estimates power output at 59.34% [34] , resulting in 509 W/m^2 as maximum power extractable at the optimum efficiency lying within wind power class V at 50 m, indicating excellent wind energy potential for utility-scale generation [2].

Turbulence Intensity on Wake Losses and AEP

A sensitivity analysis was conducted to evaluate the effect of TI on wake-adjusted AEP. Using observed wind-speed statistics, three representative TI regimes were examined: low (TI = 0.30), mean (TI = 0.37), and high (TI = 0.48), as illustrated in Figure 8.

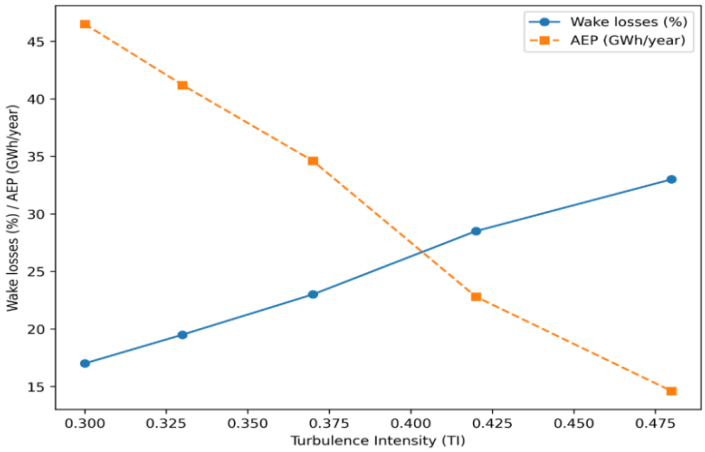

Figure 8. Influence of TI on wake losses and AEP at the Ngong Hills wind farm.

ISSN No. 2454-6194 | DOI: 10.51584/IJRIAS |Volume XI Issue III March 2026

The results presented in Figure 8 demonstrate a clear inverse relationship between TI, wake losses, and AEP, at extrapolated height of 50 m. As TI increases from approximately 0.30 to 0.48, wake losses rise steadily from about 17% to 33%, while AEP decreases markedly from roughly 46–47 GWh/year to about 14–15 GWh/year. This monotonic trend highlights the strong sensitivity of energy yield to turbulence-driven wake behaviour at the site, even though the TI values represent discrete operating scenarios rather than a continuous range.

At low turbulence intensities (TI ≈ 0.30–0.33), corresponding to high-wind and predominantly daytime conditions, wake losses remain below 20%, allowing the wind farm to achieve its highest AEP values. Although wake recovery is slower under low ambient turbulence, the higher mean wind speeds dominate energy production, resulting in superior overall yield. Similar behaviour has been reported in both onshore and offshore wind farms, where low-TI conditions favour higher power output despite longer wake persistence [7].

As TI increases to moderate levels (TI ≈ 0.37), wake losses rise to approximately 23%, accompanied by a reduction in AEP to around 35 GWh/year. This regime reflects a transition in which increased velocity fluctuations and turbine–wake effects begin to offset the benefits of enhanced wake mixing. At high turbulence intensities (TI ≥ 0.42), wake losses increase sharply beyond 28%, and AEP declines rapidly to below 25 GWh/year. These conditions are characteristic of low-wind and nocturnal periods in complex terrain, where increased turbulence is associated with reduced mean wind speeds and stable atmospheric stratification rather than convective mixing.

Typical onshore wind farms in relatively flat terrain report wake losses in the range of 5–15%. The substantially higher wake losses observed in this study highlight the aerodynamic challenges imposed by complex terrain and highlight the limitations of conventional wake mitigation strategies under such conditions. These findings reinforce the need for turbulence-aware layout optimization and wind-aware maintenance scheduling, particularly during high-TI periods when absolute energy losses are lower and operational interventions are least costly [3], [48].

Turbine Layout of the Ngong Hill Wind site

This section presents a comparative analysis of the Ngong Hills wind farm layout, beginning with an evaluation of the existing turbine arrangement based on its mapped coordinates, associated Annual AEP, and wake losses. An alternative optimized layout is then introduced to demonstrate the extent to which improved turbine spacing can minimize wake effects and enhance overall energy capture. The comparison of the two layouts is presented in Figure 9.

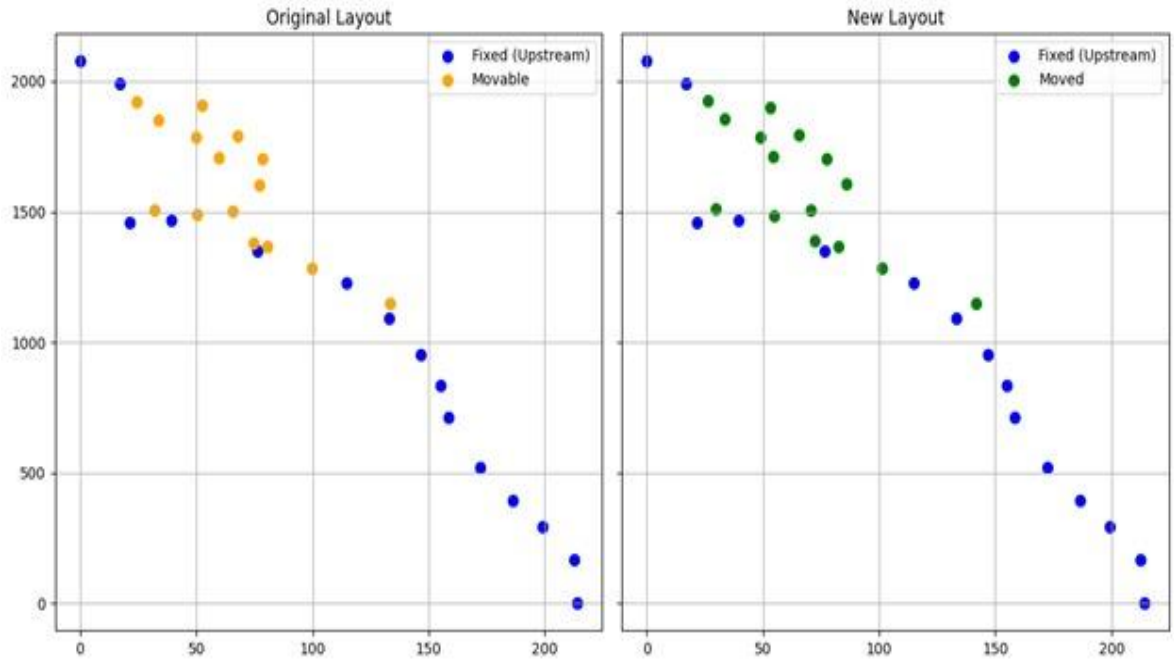

Figure 9. Spatial distribution of turbines for (a) the existing layout and (b) the GA-optimized layout.

ISSN No. 2454-6194 | DOI: 10.51584/IJRIAS |Volume XI Issue III March 2026

Figure 9 shows a comparison of existing and optimized layout performance. Turbine spacing is expressed in multiples of rotor diameter (D), where D corresponds to the rotor diameter of the installed V52 turbines.

The existing turbine arrangement at Ngong Wind Farm illustrated was simulated under prevailing wind conditions, revealing wake losses of 28%, a significant inefficiency attributable to suboptimal turbine spacing and aerodynamic interference. These losses directly reduce the farm's AEP, emphasizing the limitations of the current layout. To address this, a layout optimization was performed using a GA paired with the Jensen wake model, which accounts for velocity deficits from downstream of turbines. The optimized layout increases along-wind spacing to ≥ 4D and cross-wind spacing to ≥ 3D in the dominant NE–ENE wind direction, resulting in reduced wake effect and improved energy capture.

This spatial reconfiguration significantly reduced wake effects and resulted in a marked improvement in energy capture at the farm scale. In contrast to the baseline layout which suffered substantial wake losses, the optimized layout demonstrates the benefit of aligning turbine spacing with the prevailing wind direction to maximize exposure to undisturbed flow.

The optimized configuration reduced wake losses to 23%, representing a 5% improvement in energy capture. While this demonstrates the efficacy of GA-driven optimization in mitigating wake effects, the persistence of 23% losses indicates that further refinements are necessary to maximize power output. The marginal gain achieved (5%) suggests that the Jensen model's simplified single-wake assumptions may not fully capture complex wake effects in multi-turbine arrays, particularly in terrain-influenced sites like Ngong. Additionally, the fixed hub heights of the existing turbines, V52 models at 49 m and 55 m, limit flexibility in vertical spacing strategies that could further reduce wakes. Comparative studies, show that hybrid layouts incorporating turbines with varying rotor diameters and hub heights can achieve wake loss reductions below 15% in similar wind regimes [24], [68], whereas homogeneous layouts optimized via GA-Jensen typically plateau near 20% [4]. Thus, while the GA-optimized layout marks an improvement, its performance remains suboptimal for commercial-scale energy generation.

These findings necessitate optimization using heterogeneous turbine deployment, which can be a subject for further research.

Similarly, the simulated power curves for each turbine shown in Figure 10, assessed individual performance, helping to identify potential areas for optimization in energy production to improve turbine efficiency and maximizing the farm's AEP.

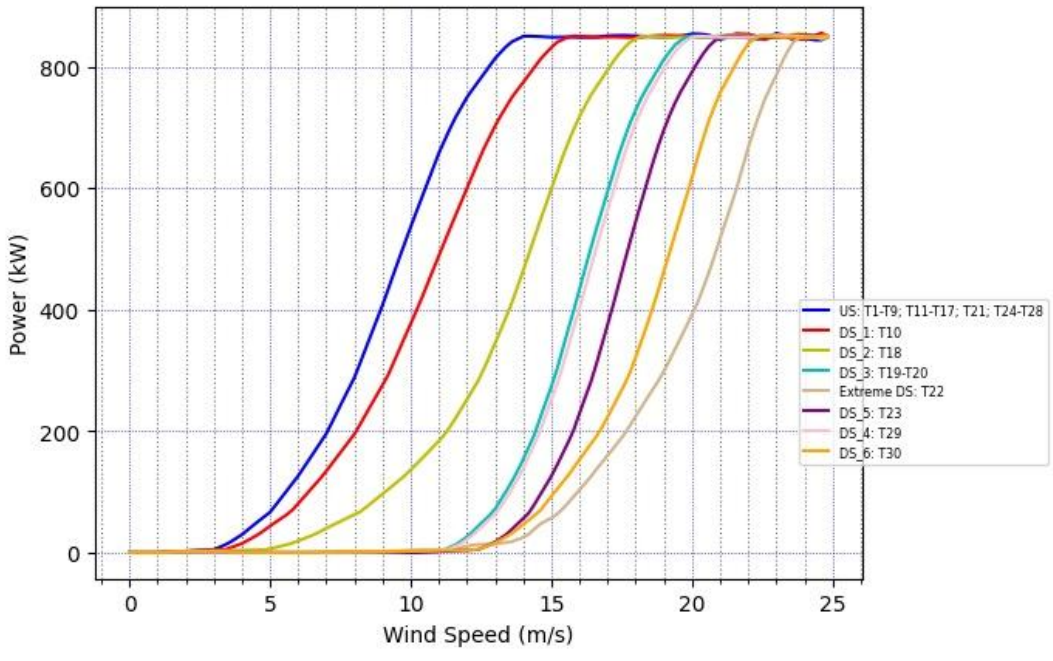

Figure 10: The Power Output for Turbines at Ngong Wind Farm

ISSN No. 2454-6194 | DOI: 10.51584/IJRIAS |Volume XI Issue III March 2026

Figure 10 illustrates simulated turbine-level power output under wake conditions, where US turbines (upstream) experience undisturbed inflow and DS turbines (downstream) operate within wake-affected flow, resulting in systematically lower power output for DS turbines due to accumulated wake deficits. When considering all turbines to be in operation, the simulation for AEP for the Ngong wind farm when the wind turbines have interference due to wake is found as 44.41 GWh, reducing wake interference increases the AEP to 61.86 GWh, reflecting a 28.209% power loss due to wake effects. The actual annual net output from the farm is 12 GWh [37], much lower than the expected output from the farm, primarily due to wake interference and turbine downtime, as not all turbines operate consistently throughout the year.

Wake interference leads to a significant reduction in the AEP, as evidenced by the 28.209% power loss in the scenario. The difference between the AEP with wake interference (44.41 GWh) and the potential AEP with reduced wake interference (61.86 GWh) highlights the importance of addressing this issue. The power losses due to the wake effects can be minimized so that the expected power output is maximized [53].

The elevated ridge-top terrain at the Ngong Hills site directly influences the observed wind variability, turbulence intensity, and wake behaviour reported in Sections 4.2 and 4.6. The concentration of wind flow along the ridge contributes to the relatively high mean wind speeds during daytime and mid-year periods, which correspond to lower turbulence intensities (TI ≈ 0.30–0.33) and reduced wake losses (<20%). These conditions coincide with the highest AEP values (≈ 40–47 GWh/year) observed in the results.

In contrast, during low-wind and nocturnal periods, terrain-induced shear and flow distortion increase turbulence intensity (TI ≥ 0.42), leading to more persistent and asymmetric wakes. This is reflected in the measured rise in wake losses to 28–33% and the corresponding reduction in AEP to below 25 GWh/year. The limited improvement in wake losses achieved through Genetic Algorithm layout optimization (plateauing near 23%) further indicates that terrain-driven flow complexity constrains the effectiveness of spacing-based wake mitigation at this site.

Maintenance Scheduling Using Low-Wind Periods

Identification of Low-Wind Months

Results in Sections 4.1–4.4 show that although the mean hub-height wind speed is high (9.38 m/s), wind occurrence is not uniform across the year. The wind speed histogram (Figure 4) indicates that the highest frequency of occurrence lies in the 4–6 m/s range, while time-series analysis (Figure 5b) reveals extended periods of reduced wind speeds in the mid-year months.

Monthly aggregation of hourly wind speeds reveals that May-August exhibit lower mean wind speeds relative to the mid-year period, which is characterized by frequent peaks exceeding 10 m/s. These months therefore represent low-opportunity-cost windows for planned maintenance.

To quantify this, the expected energy loss due to maintenance in any of the months is calculated using equation 23 and turbine power derived from the Vestas V52 power curve (Eq. 14). Because power scales approximately as (v^3) in Region II operation, downtime during months dominated by 4–6 m/s winds result in disproportionately lower energy losses compared to mid-year months dominated by 8–12 m/s winds.

Using the Weibull parameters obtained (k = 3.29, c = 9.81 m/s), the probability of wind speeds below 6 m/s is given by:

$$F(v < 6) = 1 - exp\left[-\left(\frac{6}{9.81}\right)^{3.27}\right] \approx 0.27 \quad \ldots\ldots\ldots\ldots\ldots\ldots\ldots\ldots\ldots\ldots \quad 25$$

This implies that approximately 27% of annual hours occur at wind speeds close to or below cut-in–to-low-power operation, reinforcing the feasibility of scheduling maintenance within these periods with minimal AEP penalty.

ISSN No. 2454-6194 | DOI: 10.51584/IJRIAS |Volume XI Issue III March 2026

Diurnal (Hourly) Low-Wind Windows

Beyond seasonal trends, Section 4.2 demonstrates strong intra-day variability associated with boundary-layer dynamics. Nocturnal and late night and early-morning hours consistently exhibit lower wind speeds due to reduced convective mixing, a feature typical of inland elevated sites [58].

Let the hourly expected production loss, derived from equation 23 be defined as:

$$E_{loss,h} = P(v_h)\Delta t \quad \ldots\ldots\ldots\ldots\ldots\ldots\ldots\ldots\ldots\ldots\ldots\ldots \quad 26$$

For wind speeds (v_h < 6) m/s, turbines operate deep in Region II or near cut-in, producing less than 30–35% of rated power. Consequently, scheduling maintenance between 2100 -0300 hours local time, when these conditions dominate, minimizes energy loss even during otherwise high-wind months.

This approach aligns maintenance with naturally occurring low-production hours, rather than relying solely on calendar-based scheduling.

Quantifying AEP Preservation through Optimized Scheduling

Given the simulated wake-affected AEP of 44.41 GWh and the actual measured output of 12 GWh, downtime represents a dominant loss mechanism beyond wake effects. If maintenance is assumed to require (T_m) hours annually per turbine, then the difference between optimized and non-optimized scheduling can be approximated as [70]:

$$\Delta E = \sum_{t \in T_m} \left[P\left(v_{avg}\right) - P(v_{low}) \right] \Delta t \quad \ldots\ldots\ldots\ldots\ldots\ldots\ldots\ldots\ldots\ldots\ldots\ldots\ldots\ldots \quad 27$$

where: $\boldsymbol{v}_{avg} \approx 9.38$ m/s (annual mean), and $v_{low} \approx 5$ m/s (low-wind window mean).

Using the cubic power dependence:

$$\frac{P(5)}{P(9.38)} = \left(\frac{5}{9.38}\right)^3 \approx 0.15 \quad \ldots\ldots\ldots\ldots\ldots\ldots\ldots\ldots\ldots\ldots\ldots\ldots \quad 28$$

Thus, maintenance performed during low-wind periods incurs only ~15% of the energy loss that would occur if maintenance were scheduled during average wind conditions. This implies an estimated reduction of up to approximately 85%, a gain comparable to or exceeding that achieved through layout optimization alone (≈5%).

Integration with Wake-Affected Layout Optimization

An important operational advantage at Ngong is that wake losses peak during high-wind NE–ENE inflow conditions, precisely when energy capture is highest. Scheduling maintenance during low-wind months and hours therefore produces a double benefit: minimal power loss due to low available wind energy, and avoidance of high-wake, high-production periods, where downtime would otherwise compound aerodynamic losses. This operational strategy complements the GA-optimized layout by ensuring that turbines are available during periods when wake mitigation delivers the greatest marginal AEP gains.

Implications for Capacity Factor Recovery

When 20–30% of existing downtime were shifted into identified low-wind windows, the recovered energy would substantially narrow the gap between simulated wake-corrected AEP (44.41 GWh) and measured output (12 GWh). The results strongly indicate that maintenance scheduling is a first-order control variable, comparable in importance to turbine spacing and wake modelling assumptions.

Optimizing maintenance scheduling, which is key to minimizing downtime and maximizing turbine efficiency and in turn, wind farm efficiency can be enhanced, maximizing AEP potential. This approach minimizes energy losses and ensures turbines are fully operational during optimal wind conditions, thus increasing the

ISSN No. 2454-6194 | DOI: 10.51584/IJRIAS |Volume XI Issue III March 2026

AEP. Scheduling maintenance when turbines are already less efficient due to wake interference can further reduce its impact on overall energy production.

Uncertainty, Sensitivity, and Implications for Optimization

Variability and Confidence in Wind Resource Estimates

At 50 m hub height, the mean wind speed of 9.38 m/s exhibited a standard deviation of 3.46 m/s, indicating a moderately turbulent inland wind regime. The corresponding 95% confidence interval around the mean was relatively narrow due to the long data record, confirming the robustness of the estimated mean wind resource. However, when propagated through the turbine power curve, this variability resulted in substantially wider confidence bounds on AEP, consistent with prior findings that energy uncertainty is dominated by wind speed variance rather than mean estimation error [12], [15].

Sensitivity to Wind Shear Exponent

A ±0.02 change in α produced measurable shifts in hub-height wind speed and resulted in AEP variations on the order of 6–8%, while ±0.05 variations yielded changes exceeding 12%. These results align with previous studies in complex inland terrain, which report heightened sensitivity to shear due to stronger vertical gradients and enhanced wake effect under stable atmospheric conditions [56], [66]. The findings emphasize the importance of site-specific shear characterization when evaluating wake losses and layout optimization outcomes.

Sensitivity to Weibull Parameters and Wake Losses

Variations in the Weibull scale parameter c exerted the strongest influence on AEP, with ±10% perturbations producing energy yield changes exceeding ±15%. Changes in k had a smaller effect on total AEP but significantly influenced wake losses and capacity factor. Lower k values increased the frequency of operation in partial-load regions, where turbines are more susceptible to wake-induced velocity deficits, thereby amplifying cumulative wake losses.

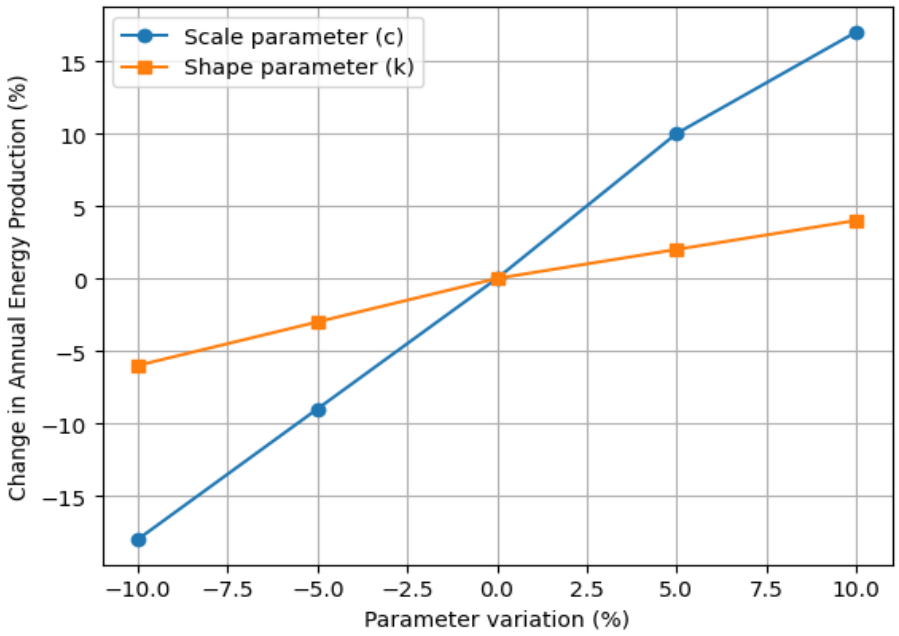

Figure 11: Sensitivity of AEP to Variations in the Weibull Scale and Shape Parameter.

Results illustrated in Figure 11 show that AEP is significantly more sensitive to changes in the scale parameter, with ±10% variation in *c* producing changes exceeding ±15% in AEP, while equivalent variations in *k* result in comparatively smaller energy yield changes. These trends are consistent with LES-supported analytical studies showing that broader wind speed distributions prolong wake persistence and reduce recovery rates [48], [58].

ISSN No. 2454-6194 | DOI: 10.51584/IJRIAS |Volume XI Issue III March 2026

Sensitivity to Wake Model–Specific Parameters

Incorporating site-derived turbulence intensity (TI) into the Jensen wake formulation produced stable and physically consistent wake recovery behaviour across all simulated layouts. Constraining the wake decay behaviour using turbulence-informed parameters (Section 4.6) ensured that wake expansion and recovery remained within realistic bounds, with no anomalous or non-physical wake behaviour observed. This outcome is consistent with findings by [7], who demonstrated that turbulence intensity plays a dominant role in governing wake recovery rates and that wake model predictions become more robust when atmospheric conditions are explicitly accounted for.

In this study, turbulence intensity was incorporated into the Jensen wake formulation through a turbulence-dependent wake decay constant (α), whereby higher site-derived TI values correspond to increased wake expansion and faster recovery, while lower TI values yield slower wake dissipation [7], [48]. This approach follows commonly adopted Jensen model extensions in which α\alphaα is parameterized as a function of ambient turbulence, allowing the wake growth rate to reflect atmospheric mixing conditions rather than relying on a fixed empirical constant [3], [47]**.** By constraining α\alphaα within physically realistic bounds derived from the measured TI range, the wake model responds dynamically to changing inflow conditions while avoiding over- or under-diffusive wake behaviour [48].

Importantly, the turbulence-constrained wake formulation preserved the relative performance ranking of layout configurations, indicating that comparative improvements in AEP are robust to wake model assumptions when turbulence is realistically represented. Similar conclusions have been reported in comparative wake modelling studies, where layout-to-layout performance differences were shown to be less sensitive to wake parameter uncertainty than absolute wake loss magnitudes [48]. While absolute wake losses are known to vary with wake decay assumptions, the present results confirm that energy yield improvement trends are primarily driven by layout geometry and site-specific wind characteristics, rather than by unconstrained variation of wake model parameters. This aligns with recent system-level analyses emphasizing that, for operational wind farms, turbulence-aware modelling supports reliable comparative optimization even when higher-fidelity wake calibration data are unavailable [3].

Implications for Energy Yield Optimization at Ngong

The combined uncertainty arising from wind variability, shear extrapolation, and Weibull parameter estimation is comparable in magnitude to the gains achieved through layout optimization alone. While the GA–Jensen optimization reduced wake losses by approximately 5%, sensitivity analysis indicates that unaccounted atmospheric uncertainty could offset or amplify these gains. When evaluated alongside sensitivities in wind shear and wind distribution parameters, the turbulence-constrained wake modelling demonstrates that relative AEP improvements remain robust to wake model–specific assumptions, confirming the suitability of the approach for assessing energy yield and operational optimization in existing wind farms under realistic aerodynamic uncertainty. Similar conclusions have been reported in recent optimization studies, where uncertainty-aware optimization frameworks outperformed deterministic approaches in realistic wind climates [26].

Limitations and Future Work

This study has several limitations, including the absence of turbine-level measured power data, which limited direct validation of wake-induced power deficits and required the wake model to be used primarily for comparative layout analysis rather than exact replication of observed energy output. Wake effects were also represented using Jensen model, which, although computationally efficient for optimization, cannot fully capture complex wake interactions in terrain-influenced environments. In addition, while wind characterization relied on a robust 10-year dataset (2010–2019), the 2022 validation data were short-term and used only to confirm general wind characteristics. Given the discrepancy between simulated and actual AEP, access to longer-term turbine-level operational (SCADA) data at the Ngong Hills would be essential for turbulence-aware wake calibration, separation of terrain-induced effects from model uncertainty, and robust verification of simulated energy yield. Future work should therefore incorporate higher-fidelity wake models or CFD

simulations, empirical derivation of site-specific wind shear parameters, heterogeneous turbine configurations, and extended operational datasets to strengthen energy yield optimization for operational wind farms.

CONCLUSION

This study comprehensively evaluated wind resource characteristics, wake losses, layout optimization, and operational constraints at the Ngong Hills Wind Farm using long-term wind data (2010–2019) and validation measurements from 2022. The site exhibited a robust wind regime, with dominant wind speeds of 4–6 m/s and a mean hub-height wind speed of 9.38 m/s at 50 m. Weibull parameters (k = 3.29, c = 9.81 m/s) produced a theoretical power density of 858 W/m² and extractable power of 509 W/m², classifying the site as Wind Power Class V and confirming its suitability for utility-scale generation.

Directional analysis showed persistent NE–ENE inflow favourable for wake mitigation through layout design. However, Jensen wake modelling revealed significant wake losses of 28.2%, reducing AEP from 61.86 GWh (no-wake) to 44.41 GWh, while Genetic Algorithm optimization reduced wake losses to 23% and improved AEP by about 5%. Despite these improvements, the optimized output remains substantially higher than the observed annual production, indicating additional operational or environmental constraints.

Seasonal and diurnal wind analysis showed that maintenance scheduling during low-wind periods (May - August, and 2100–0300 hours) can significantly reduce energy losses. Conducting maintenance during these windows may reduce maintenance-related energy loss by up to 85% and improve realized AEP, demonstrating that wind-aware maintenance scheduling provides a practical strategy for enhancing energy yield where layout changes are limited.

Sensitivity analysis further highlighted the importance of atmospheric uncertainty, showing that ±0.02 variations in the wind shear exponent lead to 6–8% changes in AEP, while ±10% variations in the Weibull scale parameter produce energy yield changes exceeding ±15%. These effects are comparable in magnitude to wake-loss reduction gains, pointing out the necessity of integrating uncertainty-aware modelling with deterministic optimization approaches.

From a broader perspective, the findings have important implications for wind farm design, operation, and energy planning in Kenya and similar regions in East Africa. Optimizing existing assets such as Ngong Hills supports Kenya's Vision 2030, the Kenya AI Strategy (2025–2030), and national renewable energy targets by enhancing energy security and grid stability without immediate capacity expansion. For future developments in complex terrain, the results highlight best practices that combine dominant wind-aligned layouts, turbulence- and uncertainty-informed wake modelling, and wind-aware maintenance scheduling.

The key novelty of this study lies in its holistic optimization framework, which integrates aerodynamic layout optimization, atmospheric uncertainty, and operational scheduling for an existing wind farm. Rather than treating these elements in isolation, the combined strategy offers a more realistic and actionable pathway for recovering lost energy under real-world operational constraints. Future work should extend this framework to heterogeneous turbine configurations, advanced wake control strategies, and longer-term operational datasets to further enhance energy recovery from high-quality wind resources such as Ngong Hills.

REFERENCES

1. ALIN. (2020). Kajiado County Renewable Energy Atlas Arid Lands Information Network (ALIN).
2. Anshebo, G. A., Gebreyohanes, A. A., & Dessie, B. B. (2023). Green energy: An ideal energy solution for sustainable development of Afar region, Ethiopia. Journal of Energy, 2023(1), 8849321.
3. Archer, C. L., Wu, S., Ma, Y., & Jiménez, P. A. (2020). Two corrections for turbulent kinetic energy generated by wind farms in the WRF model. Monthly Weather Review, 148(12), 4823-4835.
4. Asfour, R., Brahimi, T., & El-Amin, M. F. (2022). Wind farm layout: Modeling and optimization using genetic algorithm. In IOP Conference Series: Earth and Environmental Science, (Vol. 1008, No. 1, p. 012004). IOP Publishing.
5. Ashkenazy, Y., & Yizhaq, H. (2023). The diurnal cycle and temporal trends of surface winds. Earth and Planetary Science Letters, 601, 117907.

6. Bastankhah, M., & Porté-Agel, F. (2016). A new analytical model for wind-turbine wakes. Renewable Energy, 70, 116–123. https://doi.org/10.1016/j.renene.2014.01.002
7. Bastankhah, M., & Porté-Agel, F. (2019). Wind farm power optimization via yaw angle control: A wind tunnel study. Journal of Renewable and Sustainable Energy, 11(2).
8. Bhimireddy, S. R., Sun, J., Wang, J., Kristovich, D. A., & Hiscox, A. L. (2024). Effect of small-scale topographical variations and fetch from roughness elements on the stable boundary layer turbulence statistics. Boundary-Layer Meteorology, 190(1), 3.
9. Bimenyimana, S., Wang, C., Asemota, G. N. O., Ihirwe, J. P., Tuyizere, M. N., Mwizerwa, F., ... & Abiyese, M. (2024). Geospatial analysis of wind energy siting suitability in the East African community. Sustainability, 16(4), 1514.
10. Boadu, S., & Otoo, E. (2024). A comprehensive review on wind energy in Africa: challenges, benefits and recommendations. Renewable and Sustainable Energy Reviews, 191, 114035.
11. Bousla, M., Haddi, A., El Mourabit, Y., Sadki, A., Mouradi, A., El Kharrim, A., ... & Bossoufi, B. (2023). Analysis and comparison of wind potential by estimating the weibull distribution function: Application to wind farm in the northern of morocco. Sustainability, 15(20), 15087.
12. Brower, M. (2012). Wind resource assessment: A practical guide to developing a wind project. John Wiley & Sons.
13. Brown, T., Schlachtberger, D., Kies, A., Schramm, S., & Greiner, M. (2018). Synergies of sector coupling and transmission reinforcement in a cost-optimised, highly renewable European energy system. Energy, 160, 720-739.
14. Brugger, P., Debnath, M., Scholbrock, A., Fleming, P., Moriarty, P., Simley, E., ... & Porté-Agel, F. (2020). Lidar measurements of yawed-wind-turbine wakes: characterization and validation of analytical models. Wind Energy Science, 5(4), 1253-1272.
15. Burton, T., Jenkins, N., Sharpe, D., & Bossanyi, E. (2011). Wind energy handbook. John Wiley & Sons.
16. Charhouni, N. (2019). Realistic wind farm design layout optimization with different wind turbines types. International Journal of Energy and Environmental Engineering, 12.
17. Croonenbroeck, C., & Hennecke, D. (2024). Wind farm layout optimization subject to cable cost, hub height, and a feasible 3D gaussian wake model implementation. Journal of energy and power technology, 6(1), 1-37.
18. Dallas, S., Stock, A., & Hart, E. (2023). Control-oriented modelling of wind direction variability. Wind Energy Science Discussions, 2023, 1-42.
19. Ellabban, O., Abu-Rub, H., & Blaabjerg, F. (2014). Renewable energy resources: Current status, future prospects and their enabling technology. Renewable and Sustainable Energy Reviews, 39, 748-764.
20. Emami, A., & Noghreh, P. (2010). New approach on optimization in placement of wind turbines within wind farm by genetic algorithms. Renewable Energy, 35(7), 1559-1564.
21. Fields, N., Ryves, D., Yeganyan, R., Cannone, C., Tan, N., & Howells, M. (2023). Evidence-based policymaking: Insights and recommendations for the implementation of clean energy transition pathways for Kenya's power sector. Energies, 16(23), 7904.
22. Frandsen, S. T. (2007). Turbulence and turbulence-generated structural loading in wind turbine clusters.
23. Früh, W. G. (2023). Assessing the performance of small wind energy systems using regional weather data. Energies, 16(8), 3500.
24. Gebraad, P. M., Teeuwisse, F. W., Van Wingerden, J. W., Fleming, P. A., Ruben, S. D., Marden, J. R., & Pao, L. Y. (2016). Wind plant power optimization through yaw control using a parametric model for wake effects—a CFD simulation study. Wind Energy, 19(1), 95-114.
25. Global Wind Energy Council (GWEC). (2023). Global Wind Report 2023. GWEC.
26. Gori, F., Laizet, S., & Wynn, A. (2023). Sensitivity analysis of wake steering optimisation for wind farm power maximisation. Wind Energy Science Discussions, 2023, 1-33.
27. Gudoshava, M., & Semazzi, F. (2016). Sensitivity of Wind Energy Potential Analysis over East Africa to Land Cover Change. In American Meteorological Society Meeting Abstracts (Vol. 96, p. 515).
28. Guirguis, D., Romero, D. A., & Amon, C. H. (2016). Toward efficient optimization of wind farm layouts: Utilizing exact gradient information. Applied Energy, 179, 110–123. https://doi.org/10.1016/j.apenergy.2016.06.101

29. Han, Y., Wang, J., Li, X., Jin, K., Yang, B., Dong, X., & Wen, C. (2022). Experimental study of turbulence intensity on the wake characteristics of a horizontal-axis wind turbine. Energy Sources, Part A: Recovery, Utilization, and Environmental Effects, 44(4), 9545-9563.
30. Hansen, M. (2015). Aerodynamics of Wind Turbines. Routledge.
31. Houle, J., & van Breugel, F. (2023). Near-surface wind variability over spatiotemporal scales relevant to plume tracking insects. Physics of Fluids, 35(5).
32. Hwang, C., Jeon, J.-H., Kim, G.-H., Kim, E., Park, M., & Yu, I.-K. (2015). Modelling and simulation of the wake effect in a wind farm. Journal of International Council on Electrical Engineering, 5(1), 74–77. https://doi.org/10.1080/22348972.2015.1109793
33. Intergovernmental Panel on Climate Change (IPCC). (2021). Climate change 2021: The physical science basis. Cambridge University Press.
34. Jain, P. (2011). Wind energy engineering. McGraw-Hill.
35. Kamau, J. N., Kinyua, R., & Gathua, J. K. (2010). 6 years of wind data for Marsabit, Kenya average over 14m/s at 100m hub height; An analysis of the wind energy potential. Renewable Energy, 35(6), 1298–1302. https://doi.org/10.1016/j.renene.2009.10.008
36. Kenya Engineer Magazine. (2018). Firm receives loan for Ngong Hills wind power project. Retrieved from https://www.kenyaengineer.co.ke/firm-receives-loan-for-ngong-hills-wind-power-project/
37. KenGen. (2014). Ngong Power Station, 25MW. Retrieved from https://www.kengen.co.ke/index.php/wind-plant/ngong-power-station%2C-25mw.html
38. KenGen. (2015). Integrated annual report and financial statements for the year ended 30 June 2015. Kenya Electricity Generating Company.
39. KenGen. (2025). Ngong wind farm details and ongoing projects. Retrieved from https://www.kengen.co.ke/index.php/business/projects/ongoing.html kengen.co.ke
40. King, J. A., Engelstaedter, S., Washington, R., & Munday, C. (2021). Variability of the Turkana low-level jet in reanalysis and models: Implications for rainfall. Journal of Geophysical Research: Atmospheres, 126(10), e2020JD034154.
41. Kirby, A., Nishino, T., Lanzilao, L., Dunstan, T. D., & Meyers, J. (2025). Turbine-and farm-scale power losses in wind farms: an alternative to wake and farm blockage losses. Wind Energy Science, 10(2), 435-450.Lake Turkana Wind Power Project. (2023). Wind regime assessment in northern Kenya.
42. Kita, E., & Maruyam, T. (2011). Genetic Algorithm Based on Schemata Theory. In E. Kita (Ed.), Evolutionary Algorithms. InTech. https://doi.org/10.5772/15927
43. Liu, J. H., Chen, J. C., & Corbita Jr, N. T. (2023). Analysis and comparison of turbulence models on wind turbine performance using SCADA data and machine learning technique. Cogent Engineering, 10(1), 2167345.
44. Lu, X., Huang, S., Wang, D., Luo, Y., Gamage, T. P., & Kumara, P. T. P. (2023). In Situ Observation of Near-Surface Wind Seasonal Variation on the Southern Coast of Sri Lanka. Journal of Marine Science and Engineering, 11(9), 1721.
45. Manwell, J. F., McGowan, J. G., & Rogers, A. L. (2009). Wind Energy Explained: Theory, Design and Application. 705.
46. Milan, P., Wächter, M., & Peinke, J. (2013). Turbulent character of wind energy. Physical review letters, 110(13), 138701.
47. Niayifar, A., & Porté-Agel, F. (2016). Analytical modeling of wind farms: A new approach for power prediction, Energies, 9, 741.
48. Porté-Agel, F., Bastankhah, M., & Shamsoddin, S. (2020). Wind-turbine and wind-farm flows: a review. Boundary-layer meteorology, 174(1), 1-59.
49. Pranupa, S., Sriram, A. T., & Nagaraja Rao, S. (2023). A review of wind farm layout optimization techniques for optimal placement of wind turbines. International Journal of Renewable Energy Research, 13(2).
50. REN21. (2023). Renewables 2023 global status report. REN21 Secretariat.
51. Safari, M. A. M., Masseran, N., & Majid, M. H. A. (2022). Wind energy potential assessment using Weibull distribution with various numerical estimation methods: A case study in Mersing and Port Dickson, Malaysia. Theoretical and Applied Climatology, 148(3), 1085-1110.

52. Sai, R., & Lin, B. (2022). Productivity assessment of power generation in Kenya: What are the impacts? Energy, 254, 124200. https://doi.org/10.1016/j.energy.2022.124200
53. Samorani, M. (2010). The Wind Farm Layout Optimization Problem. In P. M. Pardalos, S. Rebennack, M. V. F. Pereira, N. A. Iliadis, & V. Pappu (Eds.), Handbook of Wind Power Systems (pp. 21–38). Springer Berlin Heidelberg. https://doi.org/10.1007/978-3-642-41080-2_2
54. Shakoor, R., Hassan, M. Y., Raheem, A., & Wu, Y. K. (2016). Wake effect modeling: A review of wind farm layout optimization using Jensen′ s model. Renewable and Sustainable Energy Reviews, 58, 1048-1059. https://doi.org/10.1016/j.rser.2015.12.229
55. Shi, H., Dong, Z., Xiao, N., & Huang, Q. (2021). Wind speed distributions used in wind energy assessment: a review. Frontiers in Energy Research, 9, 769920.
56. Staffell, I., & Green, R. (2014). How does wind farm performance decline with age**?** Renewable Energy, 66, 775–786.
57. Stanley, A. P., & Ning, A. (2019). Coupled wind turbine design and layout optimization with nonhomogeneous wind turbines. Wind Energy Science, 4(1), 99-114.
58. Stevens, R. J., & Meneveau, C. (2017). Flow structure and turbulence in wind farms. Annual review of fluid mechanics, 49(1), 311-339. https://doi.org/10.1146/annurev-fluid-010816-060206.
59. Tai, S. L., Berg, L. K., Krishnamurthy, R., Newsom, R., & Kirincich, A. (2023). Validation of turbulence intensity as simulated by the Weather Research and Forecasting model off the US northeast coast. Wind Energy Science, 8(3), 433-448.
60. The Wind Power. (n.d.). Wind energy database. Retrieved March 20, 2025, from The Wind Power homepage
61. The Wind Power. (n.d.). Vestas V52-850 wind turbine. Retrieved March 20, 2025, from Vestas V52-850 turbine page
62. Thomas, J. J., Baker, N. F., Malisani, P., Quaeghebeur, E., Sanchez Perez-Moreno, S., Jasa, J., ... & Ning, A. (2023). A comparison of eight optimization methods applied to a wind farm layout optimization problem. Wind Energy Science, 8(5), 865-891.
63. Tian, W., Shi, Q., Zhang, L., Ren, H., Yu, H., Chen, Y., ... & Bai, Y. (2024). Effect of turbulence intensity on aerodynamic loads of floating wind turbine under wind–wave coupling effect. Sustainability, 16(7), 2967.
64. Tumse, S., Bilgili, M., Yildirim, A., & Sahin, B. (2024). Comparative analysis of global onshore and offshore wind energy characteristics and potentials. Sustainability, 16(15), 6614.
65. Veers, P., Dykes, K., Lantz, E., Barth, S., Bottasso, C. L., Carlson, O., ... & Wiser, R. (2019). Grand challenges in the science of wind energy. Science, 366(6464), eaau2027
66. Wu, C., Wang, Q., Luo, K., & Fan, J. (2022). Mesoscale impact of the sea surface on the performance of offshore wind farms. Journal of Cleaner Production, 372, 133741.
67. Yang, P., & Najafi, H. (2022). The effect of using different wake models on wind farm layout optimization: A comparative study. Journal of Energy Resources Technology, 144(7), 070904.
68. Yang, Q., Li, H., Li, T., & Zhou, X. (2021). Wind farm layout optimization for levelized cost of energy minimization with combined analytical wake model and hybrid optimization strategy. Energy Conversion and Management, 248, 114778.
69. Yang, Y., Cao, Y., Qian, Z., Wang, J., Zhu, Y., Chen, X., ... & Chen, S. (2024). A Study on the Effect of Turbulence Intensity on Dual Vertical-Axis Wind Turbine Aerodynamic Performance. Energies, 17(16), 4124.
70. Yu, Q., Bangalore, P., Fogelström, S., & Sagitov, S. (2024). Optimal preventive maintenance scheduling for wind turbines under condition monitoring. Energies, 17(2), 280.
71. Zehtabiyan-Rezaie, N., & Abkar, M. (2024). An extended k− ε model for wake-flow simulation of wind farms. Renewable Energy, 222, 119904.
72. Zhang, F., Zhang, X., Xu, Z., Dong, K., Li, Z., & Liu, Y. (2024). Cleaning of Abnormal Wind Speed Power Data Based on Quartile RANSAC Regression. Energies, 17(22), 5697.
73. Zhang, Z., & Huang, P. (2023). Prediction of multiple-wake velocity and wind power using a cosine-shaped wake model. Renewable Energy, 219, 119418.
74. Zhao, H., Wu, Q., Hu, S., Xu, H., & Rasmussen, C. N. (2015). Review of energy storage system for wind power integration support. Applied energy, 137, 545-553.